Volcanic, tectonic and climate controls on lacustrine sedimentary supplies over the last millenia in NE Chilean Patagonia (Lake Esponja, Aysen, 45°S)

Fagel N. [1], *Pedreros P.* [2], *Alvarez D.* [2,3,] *Israde Alcantara I.* [4], *Vega Alay C.I.*[2], *Namur O.*[5], *Araneda A*[2]., *Schmidt S.*[6] *Lepoint G.*[7] *and Urrutia R.*[2]

(1) *AGEs - Clays, Sedimentary environments and Geochemistry, Department of Geology, Université de Liège, Liège, Belgium*
(2) *Faculty of Environmental Sciences and EULA - Chile Environmental Sciences Centre, University of Concepcion, Concepcion, Chile*
(3) *Centro Bahía Lomas, Facultad de Ciencias, Universidad Santo Tomás, Concepción, Chile*
(4) *Instituto de Investigaciones en Ciencias de la Tierra, Universidad Michoacacana de San Nicolás de Hidalgo. Morelia, Michoacán, México*
(5) *KUL, Leuven, Belgium*
(6) *UMR Environnements et Paléoenvironnements Océaniques et Continentaux, Université de Bordeaux, France*
(7) *Laboratory of Oceanology, Department of Biology, Université de Liège, Liège, Belgium*

e-mail address: Nathalie.fagel@uliege.be

Abstract (300 words)

The environmental variability of Northern Chilean Patagonia during the last millennia is evaluated using a multi-proxy analysis of sediment cores from Lake Esponja (45°S 72°W) to decipher if the sediment deposition is controlled by volcanic eruptions, landslides induced by earthquake or heavy rainfall. The lake is located in a glacio-tectonic valley in Patagonia. The organic-rich clayey silt sediment with low biogenic silica content was analysed for grain size, magnetic susceptibility, organic matter, biogenic silica content and diatom assemblages, mineralogy (X-ray diffraction), organic (IRMS C and N analyses) and inorganic (XRF core-scanner) geochemistry and glass shard major composition (Microprobe, SEM). The combination of ^{210}Pb, ^{137}Cs, ^{14}C and tephrochronology indicates an averaged accumulation rate of 0.4 mm/yr, leading to a record of ~3.5 kyr within 154 cm. The sedimentary geochemistry records changes in volcanic supplies, diatom productivity and detrital inputs. The sediments were interrupted by millimetric to centimentric layers corresponding to tephra deposition related to explosive eruptions of nearby volcanoes Macá, Melimoyu and Hudson.

Concerning the diatoms, the dominant planktonic species (80-150 cm) are replaced by benthic species in a transition interval (55-80 cm) and then by *Surirella spp.* in the upper core. This last genus indicates a closure of the basin ~2 ka ago, probably related to an uplift linked to a rejuvenation of the Mañihuales fault. This local change could reflect ~~more~~ regional tectonic instability. Indeed, a partial earthquake rupture occurred around ~AD100 along the southern part of the Valdivia segment, recorded as a mass transport deposit in Aysén fjord sedimentation. The fine detrital input varies over time with ~~higher~~ more variable Si/Al values in the lower part of the LEs14 core than in the upper 80 cm. The higher values may reflect wetter conditions, leading to an higher lake level and more turbid conditions in agreement with changes in diatom assemblages.

Keywords: Lacustrine sediment, sedimentary geochemistry, diatom assemblages, tephra, Late Holocene, Chile

1. Introduction

Lacustrine sediments have been widely used as a reliable archive for climatic reconstructions in particular over the Holocene (e.g. Bradley, 1999). However, the approach requires to unambiguously evidence any event deposit that interrupted the background sedimentation to elaborate a robust age model. Those events may record regional tectonic activities related to earthquakes (Chapron et al., 1999), volcanic eruptions (e.g. Naranjo and Stern, 2004; Fontijn et al., 2014), landslides or earthquake-induced landslides (e.g. Siegenthaler and Sturm 1991). They may also register climatic changes like debris flow related to heavy rainfall (Moreiras 2005; Sepulveda et al., 2006), snowmelt or even anthropogenic activities (e.g. Guyard et al., 2007; Waldmann et al., 2011).

In Chile, in particular, the Southern Volcanic Zone (SVZ) of the Chilean Andes is characterised by numerous lakes that are affected by a complex interplay of tectonics and

volcanism (Cembrano and Lara, 2009). Regional tectonic is mainly controlled by the oblique convergence between the Nazca and South American plates (Figure 1a) and the associated orogeny of the Andes (Sepulveda et al., 2006). The resulting volcanic activity comprises alignments of strato-volcanoes on ancient faults of the volcanic arc (Cembrano and Lara, 2009; Legrand et al., 2011) and monogenic cones located in the vicinity of the Liquiñe-Ofqui Fault Zone (LOFZ) (Cembrano et al. 2000). LOFZ is an active trench-linked structure associated to an intra-arc shear zone (Cembrano et al., 2000). Beside recent major seismic activity (e.g. the 1960 Great Chilean earthquake in Valdivia on May 1960 corresponding to the strongest magnitude (Mw 9.5) ever instrumentally-recorded - Kanamori, 1977; the seismic swarm (Mw 6.2) occurring in Aysen Fjord in 2007 and associated rockslide-induced tsunami - e.g. Vanneste et al., 2018), paleoseismic activities have been more and more evidenced by mass-wasting deposits in fjords and lakes from SVZ (Chapron et al., 2006; Moernaut et al., 2006; Van Daele et al., 2013; Wils et al., 2018, 2020). Most of the earthquake-induced landslides occurred along the LOFZ in the Andes (Chapron et al., 2006).

[insert Figure 1]

The aim of this study is to identify the main controls on the lacustrine productivity and sediment deposition in an active tectonic area of North Chilean Patagonia over the last four millennia. Sedimentological, geochemical and biological proxies are combined to understand the sources and origin of the particles that settle down at the lake bottom. The temporal evolution of abiotic proxies is further compared with the evolution of the biological assemblages to reconstruct the environmental conditions prevailing in the watershed. In an active tectonic area such as Patagonia, the identification of both regional and local volcanic and tectonic-related perturbations in the LEs record is a prerequisite for further paleoclimate reconstruction.

2. Study area

Lake Esponja (45°09'S, 72°08'W) is a small closed lacustrine system (0.25 km^2) located in Villa Mañihuales town (Figure 1). The lake bathymetry marked a maximum depth of 42 m. This lake is a perched lake set in a wide NNE-SSW valley extending ~60 km SW to Puerto Aysén (Figure 1a) bypassed by the west by the river Mañihuales (Figure 1b) and by the south by the river Ñireguao (Figure 1c). Mañihuales valley is of tectonic-glacial origin. The LOFZ (Figure 1a) is the main structural feature of the area (Charrier et al., 2007) corresponding to an active dextral strike-slip lineament system (Hervé 1994, Cembrano et al., 1996). The local transpressional dextral fault (i.e. called the Rio Mañihuales fault, Thomson 2002 – see location on Figure 1b), oriented NNE-SSW, is related to the overall geometry of the LOFZ fault (Figure 1a). Landslides, debris flows and local rock falls were observed in Villa Mañihuales area (see location on Figure 1c). Mass wasting was locally triggered by intense precipitations along steep slopes (SERNAGEOMIN, 2012) and they may be regionally recorded in the Aysén fjord by density-flow deposits with reworked tephra (Van Daele et al., 2013).

Besides, the watershed of the lake is in the active volcanic area of the Southern Volcanic Zone (SVZ - Stern et al., 2004). It is located east of five volcanoes (see location on Figure 1a), among them the Macá and the Hudson are the most active. The recent, historical and prehistorical eruption activity was intensively studied in particular in lake records (e.g. Haberle and Lumley, 1998; Naranjo and Stern, 2004; Watt et al., 2013; Fontijn et al., 2014; Fontaine et al., 2021). The main widespread tephra layers are related to the explosive eruptions of the Hudson, Macá, Mentolat and Melimoyu-volcanoes (Naranjo and Stern, 1998; 2004; Watt et al., 2013).

Regional geology is made by two main units (Pankhurst et al., 1999; SERNAGEOMIN, 2003). The North Patagonian batholith, on the western side, is mainly composed by Late

Jurassic/Cretaceous granites and granodiorites (Figure 1b). On the eastern side continental Mesozoic volcanic sequences are intercalated with some sedimentary marine deposits. The Late Jurassic Ibañez Formation is made by dacitic to rhyolitic lavas and pyroclastic deposits and the Early Cretaceous Divisadero Formation by andesitic to rhyolitic lavas and tuffs. Quaternary and Plio-Pleistocene alluvial deposits, morainic and fluvio-glacial deposits occur along rivers.

Patagonia is located within the mid-latitude 30-60°S belt, between the Intertropical Convergence Zone to the North and the Antarctic Convergence Zone to the South. Its climate variability over the Holocene is mainly controlled by the intensity and /or latitudinal position of the Southern Westerlies Winds (SWW) (e.g. Markgraf 1993, Gilli et al., 2005). Some authors suggested millennial changes in the strength of the SWW since the last glaciation without major latitudinal migration (Villa-Martinez et al., 2012), other ones rather proposed a latitudinal migration of SSW over the Holocene (Markgraf et al. 2003, Bertrand et al. 2014, Perren et al. 2020). At present, SWW bring heavy precipitation over the western side of southern South America but generate arid conditions on the eastern side of the Andes (Garreaud, et al., 2013).

The regional climate is humid and temperate with rainy winter and short dry mild to cold summer, corresponding to the class Cfb to Cfc of the classification of Köppen (Peel et al., 2007). The meteorological station of Villa Mañihuales (45° 10’ 27.45” S, 11° 72°8’52.58” E) reports an annual average of cumulated precipitation of 1484 mm ± 367 and temperature of 9.2°C ± 0.6 between 1986-2013 interval (Data from DGA). The warmest month (February) is characterized by an average temperature of 14.6°C ± 1.7 and low averaged precipitation (60 mm ± 42). The wetter month (June) presents an average precipitation of 198 mm±103 and cold temperature (4.2°C±1.3). The vegetation corresponds to an intermediate ecotone, comprised between the western humid zone and the eastern steppic zone, characterized by

forest of *Nothofagus pumilio* (Lenga beech) (Luebert and Pliscoff, 2006; Hepp et al., 2018). During the twentieth century the forest has been strongly reduced by human-induced fires and replaced by herbaceous species to produce grasslands in the valley (Bizama et al., 2011).

3. Material and methods

3.1.Sedimentological and biological analyses

Three cores LEs11A (109 cm), LEs13 (23.5 cm) and LEs14 (155 cm) were collected using an Uwitec® gravity corer during different fieldtrips in 2011, 2013 and 2014, respectively~~in the deepest part of the lake~~. LEs14, i.e. the main core investigated in this study, was retrieved in the deepest part of the lake (42 m) at 45°09'54.3" latitude S and 72°08'55.9" longitude W (Fig. 1C) whereas the two other cores were retrieved at 40 m depth. The core LEs13 was cut at 5 mm for geochronological purpose. The cores LEs11A and LEs14 were cut longitudinally. One half-core section (i.e. archive section) was described, photographed and measured by magnetic susceptibility (MS) with a Bartington® magnetic susceptibility meter MS2E point sensor with a 5 mm sampling interval. The correlation between the cores LEs11A and LEs14 is reported at SM Figure 1. For LEs14, the half-core working sections were further subsampled into 25 cm long x 4 cm wide x 1.5 cm deep aluminium boxes. The remaining sediment material was subsampled at 2.5 cm for organic content measurements by Loss-On-Ignition (LOI) (Heiri et al. (2001).

[Insert SM Figure 1]

The sediment grayscale levels and XRF elemental core scanning were measured using a Scopix X-ray image-processing system (58kV, 10mA) and an Avaatech XRF core scanner with a Fe-Mo tube at the EPOC laboratory (Université de Bordeaux, France). The measurements were performed on the aluminium boxes. The XRF core scanning was done for 15 elements (i.e. from Al to Ba) at 10, 30 and 50KV and 15, 20 and 25s exposure time,

respectively. Elemental ratios of Zr/Rb, Ca/Ti, Br/Ti and Si/Al were tested to reconstruct the grain-size and/or the origin of the sedimentary supplies (Wang et al., 2011; Kylander et al., 2011; 2012; Kalugin et al., 2013; Carrevedo et al., 2015).

To complete the sedimentological description, grain-size data were determined at a sampling resolution of 2 cm for LEs14 (n=79). Grain-size analysis was performed by a laser Malvern® Mastersizer 2000 diffraction particle analyser at the ARGENCO Department (Université de Liège). The bulk sediment samples were sieved at 2 mm, dispersed in deionised water and introduced into the Hydro 2000G dispersion unit. The sample amount was adjusted to reach an optimal laser beam obscuration of 15% ±5. The sampled was then homogenised with a 2000 rpm stirrer and disaggregated with 20% of ultrasonic waves. The analysis was triplicate to ensure the reproducibility of the data. The grain-size parameters (i.e. mean and percentile) were calculated according to Folk and Ward (1957).

The mineralogical phases were identified by X-ray diffraction (XRD) on LEs14 (n=27) with an averaged sampling step of 10 cm. Some additional samples were selected on coarse layers in LEs 14 and from the main tephra layer of LEs11 to confirm the presence of glass phases. The 40°C-dried and crushed < 150 microns sediment sample powder was measured by the backside method described by Moore and Reynolds (1997). The non-oriented powder was scanned from 2 to 70° 2θ with a step size of 0.009°2θ, and a time per step of 0.5 seconds with a Bruker® D8-Advance Eco diffractometer (Cu Kα radiance, λ=1.5418Å, 40 KV, 25 mA) coupled with a Lynxeye Xe detector. The presence of a glass phase was deduced from the intensity of the diffraction band at 4.04Å that corresponds to the total amorphous content (i.e. sum biogenic silica, volcanic glasses and organic matter) (Fagel et al., 2017).

The glass shard major element chemistry was analysed on the coarsest silty and sandy layer in 14 samples in LEs14 and 3 samples retrieved between 68 and 78 cm in LEs11. The glass shards were extracted following the protocol of Lowe (2011). An aliquot of bulk

sediment samples (~0.8 to 2.4 g) was dry sieved at 80 µm. The < 80 µm fraction was leached by adding 0.5 ml of concentrated acids HNO_3 14N and HCl 6N at 25°C for 15 minutes. The solid residue was rinsed three times by deionized water, dried at 40°C overnight before a liquid density separation. Bromoform was added to the dried residue for a 30 min. centrifugation at 4000 rpm. The tube was frozen dry by liquid nitrogen and the supernant was retrieved with acetone. The dried lighter fraction was mounted in epoxy resin for analysis by Electron Probe Micro-Analyzer (EMPA) with a Cameca SX5 FE at the Rurh-University of Bochum (Germany). The analytical conditions were set at 15 kV and 8 nA with a beam size of 5 to 15 µm (more detailed analytical protocol see Oladottir et al., 2011). For calibration of the Kα X-ray lines, we used the following standards: albite (Al, Na), orthoclase (K), wollastonite (Si, Ca), TiO_2 (Ti), Fe_2O_3 (Fe), MgO (Mg), and Mn_3O_4 (Mn). Counting times were 10 seconds on peak and 5 seconds on background on either side of the peak. During analytical session the international glass standards A99 and VG2 were used as external standards to monitor the accuracy of the analyses and compare them with published values (Oladottir et al., 2011). In the following text, the tephras are labelled as T1 to T11 according to the stratigraphical order, T1 being the youngest layer.

For diatom analysis, sediment samples were taken at 2 cm intervals in LEs14 (n=68). A subsample of 0.5 g of sediment were treated with HCl and H_2O_2 to remove carbonate and organic matter, respectively. For microscopic analysis an aliquot of 4 microliters was dried on a cover adding a mountant medium (Naphrax) on a microscope slide (Battarbee et al., 2001). A minimum count of 500 valves were carried out for each sample, except for diatom poor samples where only 100 valves were counted. Diatom were identified to species or genus level using the taxonomic references from Morales et al. (2014), Krammer and Lange-Bertalot (1986, 1988, 1991a, 1991b), Hartley et al. (1996), Lange-Bertalot et al. (2000). To distinguish different association in the sediment core, a stratigraphically constrained sum-of-

squares cluster analysis (CONISS) were performed with Tilia software (Grimm 1991). Only diatoms with an abundance of >5% were plotted.

C/N ratio were measured at 1 cm sampling resolution for LEs11 (n=69) following the protocol of Hedges and Stern (1984). A few samples were also analysed in LEs14 (n=23) in order to compare their values with LEs11. The dried sediment sample was crushed by hand in a mortar and then treated with HCl to remove any carbonates. About 25-30 mg of sediment sample was analysed for C/N ratio at the Laboratory of Oceanology (Université de Liège, Belgium) with a Vario MicroCube elemental analyser coupled with a mass spectrometer Isoprime 100.

Complementary analyses of biogenic silica were measured by successive leaching procedures on ~50 mg of dried bulk sediment of LEs11 (n=35) at a sampling resolution of 2 cm, except in the coarsest layer (53-78 cm). The organic fraction was removed by addition of H_2O_2 10%, the carbonate fraction by HCl 1N and then the total silica fraction by NaOH 0.2N (Olhendorf and Sturm, 2008; Carter and Coleman, 1994). Al and Si contents were measured by Atomic Absorption using a spectrometer Analytikjena NovAA 300 (Department ARGENCO, Université de Liège) calibrated with artificial solution (50 to 200 mg/l for Si, 25 and 100 mg/l for Al). The detrital silica content is derived from a normative calculation (Leinen, 1977) using the measured Al content and the averaged Si/Al ratio (0.93) of four soil samples collected in the lake catchment. The estimated biogenic silica content corresponds to the measured total silica content minus the calculated detrital silica.

3.2. Core chronology

The ^{210}Pb, ^{226}Ra, ^{232}Th and ^{137}Cs data were measured with a 5 mm resolution in the upper 16 cm of core LEs13. The measurements were done with a low-background and high-efficiency gamma detector in the laboratory EPOC (Univ. Bordeaux, France). The ^{226}Ra content was removed from the ^{210}Pb content to calculate the excess ^{210}Pb activities (i.e.

$^{210}Pb_{xs}$), further converted into age by using the Constant Flux/Constant Sedimentation model (CF/CS - Appleby and Oldfield, 1978). The peak of ^{137}Cs activity was used as independent chronological marker, where its maximum activity is recorded around 1965 (Stupar et al., 2014). Ages from ^{210}Pb chronology in LEs13 were correlated with LEs14 using the magnetic susceptibility profiles of both cores.

Radiocarbon dates were measured on bulk sediment or macroremain at the Gadam Laboratory from the Silesian Institute of Technology (Gliwice, Poland). Because ^{14}C dates can be affected by dissolved organic carbon derived from soils (Grimm et al. 2009), an age correction was applied to the bulk sediment according Bertrand et al. (2012), who proposed to estimate the influence of organic matter input from the watershed on bulk radiocarbon ages using the measured atomic C/N ratios of lacustrine sediments. Defined from four lake sedimentary records from north Chilean Patagonia, such approach that allows to derive a reservoir age for bulk sediment is at least valid at the regional scale. The ^{14}C results were then calibrated using the Southern Hemisphere calibration curve (i.e. SHCal13 - Hogg et al., 2013). Dates from ^{210}Pb and ^{14}C were integrated in the age-depth model for LEs14 by Bayesian model using R software packages Bacon 2.5.3 (Blaauw et al., 2021). The followed methodology, even imperfect due to complex carbon cycle in volcanic lakes (Frugone-Alvarez et al., 2020), allow to estimate the age of the sedimentary record that will be further constrained by the tephrostratigraphy.

3.3. Statistical analysis

Multivariate analysis was performed on the XRF dataset using R software (R Development Core Team, 2018) and its *rgr* (Garrett, 2018) and *pcaPP* packages (Filzmoser et al., 2018). The geochemical data were centred log-ratio (clr) transformed prior to a Robust Principal Component Analysis (RPCA - Candès et al., 2011; Croux et al., 2013). This transformation is useful for this type of data, since it conserves all the elements, which facilitates the

interpretation of the associated geochemical processes (Aitchison, 1986; Mueller and Grunsky, 2016). RPCA was chosen because it has been successfully applied on high resolution XRF data characterized by numerous outliers (Frugone-Álvarez et al., 2017; Żarczyński et al., 2019). Only the Principal Components (PC) with eigenvalues > 1.0 were retained as significant for the total variance of the dataset (Davis, 2002).

To identify any climatic control, the geochemical ratios were compared to the precipitation data by a correlation matrix applied moving average filters of three, five and seven years for the period AD 1930 to 2014. The precipitation reanalysis data set of the CRU_TS 4.03 (Harris and Jones, 2020) were retrieved for an area comprised between latitude 45-45.5°S and longitude 72-72.5°W (http://climexp.knmi.nl). Prior, the CRU_TS data set was correlated with local (Villa Mañihuales) and regional (Puerto Aysen) instrumental precipitation data to validate the reanalysis data. May and June cumulated precipitation was used because it was the longest precipitation record to obtain a robust statistical analysis. The meteorological station of Villa Manihuales displays similar temporal trend with the regional station of Puerto Aysén (45°23'57.98"S, 72°40'37.99"W), giving for instance a Pearson correlation for accumulated May to June precipitation $r_{p\ MMJ} = 0.73$ $p < 0.001$. (data Puerto Aysén 1960-2017 from INIA report - Hepp et al., 2018). The instrumental measurements of Villa Manihuales were then correlated with climate reconstruction CRU_TS 4.03 (Harris and Jones, 2020) in order to extend the calibration period to the whole twentieth century ($r_{annual\ precipitation} = 0.72$ $p < 0.001$).

Changes in the diatom assemblage over time was evaluated by a Detrended Correspondence Analysis (DCA) (Hill and Gauch, 1980). Only the scores of the axis 1 were plotted against the diatom assemblages in order to study the species turnover between samples. This analysis was performed in the R software (R Development Core Team 2018) using the vegan and rioja packages (Juggins, 2017; Oksanen et al., 2019).

4. Results

4.1.Sedimentology

Macroscopic observation, grain-size distribution and grey-scale levels allowed to identify three main sedimentological units in LEs14, a detailed sedimentological description is given at Figure 2. The unit 1 (100-154 cm) is characterized by finely laminated light brown to dark brown organic-rich clayey silts (mean 10 µm, 78% 2-63 µm). A pluricentimetric homogeneous clayey interval with an upper lighter lamination is observed between 130.6 and 136 cm (reported as fine layer FL1 on Fig. 2). A similar but thinner interval is also observed between 126.9 and 128.2 cm (FL2 on Fig. 2). Unit 2 (60-100 cm) is made by diffuse laminations with similar silty grain size (mean 13 µm with 74% 2-63 µm) but lighter in colour than unit 1. An homogeneous clayey layer is evidenced between 92.3 and 98.3 cm (reported as FL3 on Figure 2). In the upper part of unit 2, a darker sandy interval (coarse layer CL on Figure 2) is evidenced between 60 and 65 cm, with 82% ±2.8 of sand. Its high ϕ50 value (228 µm ±129 – see data on Figure 2) contrasts with the ϕ50 values of the other coarse layers, recording an abundant fraction of medium sand (45% ±3 of 250-500 µm fraction). Unit 3 (0-60 cm) displays coarse millimetric to centimetric laminations between yellowish brown to dark brown clayey silts (mean 42 µm, 63% 2-63 µm). It contains a coarser light grey to dark grey layer between 39.5 and 49.5 cm composed of angular particles of various sizes (mean 31 µm, 49% 2-63 µm, ϕ50 55 µm ±31). This layer (labelled as T5) is overlaid between 29.6 and 39.5 cm by darker and diffusely laminated coarse silts to sands (mean 38 µm, 56% 2-63 µm, 39% > 63 µm, ϕ50 39 µm ±41).

[Insert Figure 2]

In addition to the darker layers at 39.5-49.5 cm (labelled T5, see below) and at 60-65 cm (CL), the sedimentation of core LEs14 is interrupted by 10 dark gray plurimillimetric fine sands observed at 13.2-13.5, 18.2-18.4, 31.5-31.7, 34.8-35, 60.7-61, 67.8-68, 81.9-82.3,

102.6-102.9, 110.7-111 cm and 148.6-148.8 cm (Figure 2). Those sandy layers (27 to 85% > 63 µm, 159 µm ≤ ϕ90 ≤ 546 µm) were characterized by higher value in magnetic susceptibility by comparison to the background value and were interpreted as tephra layers. The two homogeneous pluricentimetric clayey layers FL1 and FL3 were interpreted as fine turbidite deposits, a sedimentation process often observed in the deepest area of lake, in particular in Chile (e.g. Moernauts et al., 2014; Van Daele et al., 2015). The thinner layer FL2 is probably also associated to a similar process.

The bulk mineralogy (Figure 3) is composed by both crystallised and amorphous phases. The main minerals are clay minerals (29% ±18), quartz (16% ±11), plagioclase (25% ±16) and pyroxene (3.4% ±1.7). Amphibole (< 1%) and olivine (< 6%) are also detected in some samples. The sum of amorphous phases reaches ≥ 50% in the coarse interval 60-65 cm whereas it represents only 1% at 66-67 cm. Amorphous phase is made by at least 80% of volcanic glasses in the layers identified as tephra. Unit 1 is on average composed by detrital-derived components with 39% of clays, 21% of quartz and 5% of organic matter. The mean abundance of volcanic glasses (12%) and plagioclase (19%) is less abundant than in the lower units. Unit 2 is enriched in both volcanic glasses (30%) and plagioclase (28%) but depleted in clays (22%) and quartz (13). Unit 3 displays an averaged composition close to Unit 2, with more clay minerals (27%) and lower volcanic glasses (24%).

[Insert Figure 3]

SEM imaging of the samples together with EPMA analyses confirms the presence of numerous volcanic shards. Figure 4 presents the average SiO_2 *vs.* K_2O compositions of the glass shards along with their standard deviations (data in Table 1). Major composition of studied samples overpasses a wide range of silica content from basalts to dacites. Most samples range from intermediate calc-alkaline to K-rich siliceous andesites. The average compositions of the decimetric tephras observed in both cores LEs11 (53-78 cm) and LEs14

(39.5-49.5 cm, labelled as T5) are relatively similar and correspond to calc-alkaline intermediate andesite to siliceous andesites. The average composition of the glass shards (n= 27) measured in 3 samples from LEs11 (i.e. 67-68, 73-74 and 77-78 cm) is 66.21±5.38% of SiO_2 and 1.55±1.27% of K_2O. The silica content of the sample LEs14 48-49 averages 63.0±5.27% of SiO_2 and 1.49±0.26 % of K_2O (n= 11).

[Insert Figure 4]

[Insert Table 1]

In LEs14, the other plurimillimetric tephra layers are clustered in two main groups (K-rich group and K-poor group) according to their potassium content (Figure 4). (1) Within the K-rich group, sample 148-149 (T11) displays the highest K_2O values (2.5-2.7%) and plots within the field of K-rich calc-alkaline siliceous andesite. Sample 60-61 (T6) shows the largest chemical variability in the field of andesites (SiO_2 55.44±1.94%, K_2O 1.41±0.28%). The sample 82-83 (T8) falls within the fields of basalt to basaltic andesite with an average K_2O content of 1.50±0.24% for 55.23±1.31% of SiO_2. (2) Within the K-poor group, samples 31-32 (T3), 34-35 (T4), 102-103 (T9) and 110-111 cm (T10) display a narrow range of silica-poor glasses (53-56%) with ≤ 1.2% of K_2O, i.e. all plotting into the field of intermediate andesite. The composition of samples 13-14 (T1) is clustered within the field of siliceous andesites with 1.2±0.27% of K_2O whereas sample 18-19 (T2) is more scattered from andesite to dacite with 1.68±0.42% of K_2O for 66.2±3.2% of SiO_2. Sample 67-68 (T7) plots at the limit between calc-alkaline intermediate andesite and K-rich calc-alkaline siliceous andesite (SiO_2 66.2±3.2%, K_2O 1.03±0.34%).

The measured C/N (%) ratios are close in LEs11 and in LEs14 with a mean value of 12.7±1.4 and 12.84±1.86, respectively. A pronounced peak in C/N (15) is observed at 66-67 cm in LEs14, below the coarse layer interval (CL, Figure 2). The averaged organic matter content was estimated at 3.3%±1.6 by LOI in LEs14, with the highest values measured in unit

1 (4.8%±0.4) and the lowest values (0.6%±0.4) in the coarse layer (Figure 2). Note LOI-deduced organic matter values were lower than the estimations based on the abundance of carbon measured by optical Mass Spectrometry. Assuming 50% of carbon in organic matter, the averaged organic matter content in LEs14 evolves from 7.9% ±3.6 in unit 1, 3.8% ±2.3 in unit 2 to 8.8% ±5.7 in unit 3 (core average 7.11±4.1), the highest value (13.2%) being observed at 30-31 cm.

4.2. Core chronology

The age model of core LEs14 is reported on Figure 5. It integrates the surface age, ^{210}Pb ages estimates from CF/CS model in LEs13 and 3 calibrated and reservoir-corrected ^{14}C dates from LEs14 (Table 2). The 11 tephras layers (T1 to T11) and the three homogeneous clayey layers capped by a thin lighter layer (FL1 to FL3) were considered as instantaneous deposits in the Bacon age model.

For the upper core section, the ^{137}Cs data confirm the $^{210}Pb_{xs}$ age model (Figure 5a). The maximum ^{137}Cs activity (42 mBq/g) observed at 4.5 cm in LEs13 corresponds to an age of 1965±6.5yr AD according to the CF/CS $^{210}Pb_{xs}$ age, i.e. an age consistent with the highest period of nuclear tests in the Pacific Ocean (Stupar et al., 2014). While in the lower core section, two over the four calibrated ^{14}C ages were used, because the sample 104-105 cm and 151-152 cm were considered as outliers (Figure 5b). Even after a correction of the reservoir effect derived from C/N ratio, there is still a significant difference with the closest age-control point at 107-108 cm obtained from a macroremain (wood fragment). This observation suggests that the reservoir correction applied on bulk sediment is not sufficient due to high supplies of old carbon from the watershed of old organic matter in the lower part of LEs14 (average C/N ratio ~15 for the lower core section - see Figure 2). The Figure 5b compares two age models, with and without considering in account the two ^{14}C ages obtained on bulk sediment at 104.5 and 152.5 cm. Without considering the ages measured on bulk sediments,

the Bacon age-depth model indicates that core LEs14 covers ~ 3.5 kyr within 154 cm, with an averaged sedimentation rate of ~0.4 mm/yr, reaching up to 0.6 mm/yr for the upper 10 cm. This age model is consistent with the interval cover by LEs11 estimated from one ^{14}C date measured on a bivalve shell (*Diplodon chilensis*) retrieved between 84 and 86 cm (Table 2). Not including the three coarse intervals at 11-11.5 cm, 15-16 cm and 53-78 cm considered as tephra deposition the calibrated age of 113-235AD suggests an averaged sedimentation rate of 0.4 mm/yr. By extrapolating this sedimentation rate, LEs11 encompasses ~2 kyr within 94 cm. Such age supports the youngest sequence covered by LEs14 based on the correlation between the two cores LEs11 and LEs14. Note this age model will be further supported by tephrostratigraphy (see section 5.2).

[insert Figure 5a]

[insert Figure 5b]

[insert Table 2]

4.3. Biogenic silica and diatoms assemblages

Microscope counting in LEs14 evidences an overall low diatom abundance in Lake Esponja, confirmed by the low biogenic silica content of 5% ±3 estimated by leaching method in LEs11 (data reported on SM Figure 1). Nevertheless, LEs14 is characterized by an important diversity in the benthic diatoms with 23 genus and 153 species whereas only two genera of planktonic diatoms were observed.

The DCA results indicated three principal periods of the diatom assemblage: DZ1 (150-80 cm; 1.4 kyr BC to 200 BC), DZ2 (80-55 cm; 200 BC – 316 AD) and DZ3 between 55-0 cm (~316 AD to present), subzones inside of these was defined by CONISS and showed in figure 6. The main change observed in DCA was associated with the replacement of planktonic and tycoplanktonic diatoms, such as *Cyclotella* sp, *Aulacoseira* spp and *Staurosira construens*, to benthic diatoms such as *Frustulia* sp and *Surirella* sp (Figure 6).

[insert Figure 6]

The DZ1 was dominated by planktonic species (i.e. *Aulacoseira* and *Cyclotella*) and tycoplanktonic genera (*Staurosira*) with low relative abundance (< 20%) of benthic genera (i.e. *Surirella*, *Gomphonema*, *Cymbella* and *Stauroneis*). The planktonic taxa were progressively replaced by two benthic genera *Frustulia* and *Surirella* in a transition interval (DZ1b 100-80 cm). The intermediate interval (DZ2 80-55 cm) showed low taxa richness (n = 31 ± 46) and was dominated by benthic genera, such as *Surirella* (< 80%), *Cymbella* and *Eunotia*, the latter with relative abundances of less than 20%. A few planktonic diatoms *Aulacoseira* were observed in one sample (62-65 cm) retrieved in the coarse sandy layer CL (60-65 cm). DZ3 zone (55-0 cm) was characterized at the base by a tephra deposit (Tephra 5). This volcanic activity caused a slight change in the relative abundance of the taxa but it did not affect the taxonomic composition of the assemblage. The diatom assemblages of DZ3 was dominated by the benthic genera *Frustulia* (≤ 60%) and *Surirella* (20-80%). The planktonic *Aulacoseira* was also well represented (< 40%), but with percentages remaining variable throughout the zone. DZ3 was also characterized by diverse benthic taxa than were minor represented or absent in the DZ1 and DZ2 zones including *Eunotia*, *Stauroneis*, *Cymbopleura*, *Gomphonema* and *Stenopterobia*. This was observed especially in the upper 25 cm.

4.4. Sediment geochemistry

The RPCA was performed on 12 elements since Mn, Y and Ba registered insignificant communalities < 0.5. The first two PC were highly significant with a cumulated variance of 88.56 % (PC1 56.7%, PC2 31.86%). In the PC1-PC2 biplot diagram (SM Figure 2), the elements were clustered in three groups (see the correlation matrix given as supplementary material SM Figure 3). Al, Si, K and Rb (group 1) plot along positive PC1 axis whereas Ti, Ca, Sr and Zr (group 2) and Mn, Fe, Zn, S and Br (group 3) were rather aligned along the PC2 axis with negative or positive value, respectively.

[Insert SM Figure 2]

[Insert SM Figure 3]

5. Discussion

The section is divided into three sub-sections. (1) The multivariate PCA analysis will allow to identify the different types of sedimentary components that settle down at the bottom of the Lake Esponja. (2) Chemical microprobe and SEM/EDS analyses of glass shards will be used to confirm the presence of tephra layers in its sedimentary record and to correlate them to past known eruptions of the regional volcanoes and lacustrine tephra records. (3) Combined with the geochemical data, the diatom assemblages will be interpreted in terms of water column conditions in relation to local or regional perturbations in the watershed induced by either volcanic, tectonic or climate changes. An overall reconstruction of the paleoenvironmental evolution of Lake Esponja setting will be proposed for the last 3.5 millennia based from both geochemical and biological proxies.

5.1. Identification of sedimentary components

The RPCA analysis applied on the geochemical sedimentary composition of Lake Esponja evidences marked changes in the sedimentary supplies in relationship with detrital and volcanic inputs. The analysed geochemical elements were clustered in three groups in the binary PC1-PC2 diagram (SM Figure 2). The RPCA correlation matrix on XRF core scanner dataset of core LEs14 is given on SM Figure 3.

In the first group aligned along PC1 axis, the Pearson correlation between Rb and K (r= 0.72 - SM Figure 3) indicates a control by fine detrital supplies enriched in clay minerals and K-feldspars (Kylander et al., 2011). Likely, the correlation between Al and Si (r= 0.92 - SM Figure 3) evidences a dominant detrital origin for Si, consistent with the low abundance of diatoms in the sediment.

Among the group 2 the relationship between Ca and Sr (r= 0.87 - SM Figure 3) is indicative of the presence of plagioclase, i.e. the dominant mineral observed in the tephra layers. Zr that is correlated to Sr (r= 0.53 - SM Figure 3) and Ti (r= 0.50 - SM Figure 3) is often related to coarse-grained fractions (Kylander et al., 2011) and/or to volcanic assemblages (Davies et al., 2015).

In the group 3, the highest correlation was observed between Br and S (r= 0.80 - SM Figure 3) and S and Zn (r= 0.73 - SM Figure 3). As those elements are often related to organic matter content (Ziegler et al., 2008), the group 3 mainly represents the supplies of allochthonous organic matter by physical weathering and erosion in the watershed. PC1 is therefore indicative of fine detrital supplies whereas the PC2 rather correspond to coarser supplies.

5.2. Identification of volcanic supplies

Quaternary volcanoes of SVZ show a close relationship with NE-striking tension cracks and with WNW striking basement faults of the Liquiñe-Ofqui system (e.g. Cembrano and Lara, 2009). The Lake Esponja is located at ~70 km East of volcanoes Cay and Macá, 120 km SE of volcano Mentolat, 134 km SSE of volcano Melimoyu and ~70 km NE of volcano Hudson. The lake may be affected by pyroclastic falls mainly from Cay or Macá (> 10 cm) and from Mentolat (~10 cm) and in a lesser way by Hudson (<10 cm) (SERNAGEOMIN, 2012; Watt et al., 2013). The stratovolcano Cay (45°03′S, 72°59′W, 2090 masl), is of one of the large composite central volcanoes in SVZ, (i.e. the closest of Lake Esponja) probably still active but it has no record of past eruptions (Naranjo and Stern, 2004). The Macá volcano is a large active stratovolcano (45°06′S, 73°10′W, 2960 masl) with only one known post glacial explosive eruption MAC1 at 550 ± 60 AD (Naranjo and Stern 2004). The Mentolat volcano (47°42′S, 73°04′W, 1660 masl) had one eruption MEN1 at 5.5 ka BC (Naranjo and Stern, 2004; Watt et al., 2013). The Melimoyu volcano (44°08′S, 72°88′W, 2400 masl) is a large

volcano covered by a glacier that had two major known eruptions, i.e. MEL1 at ~880BC year and MEL2 at ~330AD year (Naranjo and Stern, 2004; Watt et al., 2013). However, its eastern tephra dispersion rules out any influence on Lake Esponja (Weller et al., 2014). The active basaltic-dacitic volcano Hudson (45°54′S, 72°58′W, 1905 masl) has two prehistorical eruptions *ca.* 1875 ka ±235 BC (H2 3.6 ^{14}C kyr BP, Naranjo and Stern 2004) and ~ 5.8 ka BC (H1 7.43 ^{14}C kyr BP - Naranjo and Stern, 1998; Watt et al., 2013).

SVZ volcanoes fall into three chemical groups, reported in Stern et al. (2015), distinguished by their different concentrations of the incompatible elements like K_2O (Figure 4). Hudson and Melimoyu volcanoes are characterised by High Abundance magma (HAMF - López-Escobar et al., 1993, 1995a; Naranjo and Stern, 1998, 2004; Kratzmann et al., 2010) while Maca, Cay and Yanteles stratovolcanoes are Low Abundance volcanoes (LAMF - López-Escobar et al., 1993, 1995; D'Orazio et al., 2003; Gutiérrez et al., 2005). The Mentolat volcano falls in the field of Very Low magmatic Field (VLMF) with lower K_2O content at any given content SiO_2 (López-Escobar et al., 1993; Naranjo and Stern, 2004; Watt et al., 2013). Very Low Abundance centers are characterized by the presence of amphibole in their eruptive products (López-Escobar et al., 1993, 1995; Sellés et al., 2004; Watt et al., 2013).

The age of each tephra layer identified in the sedimentary records of LEs14 has been deduced from the age model to identify any correlation with the known Holocene eruptions of the surrounding volcanoes (Table 3). The main decimetric tephra layer observed in LEs14 is attributed to the Macá eruption MAC1 according to both its age and chemical composition. In LEs14, the age model suggests a median age of 537 AD (357-814 AD) for the main tephra layer T5. This age is consistent with the youngest age of the Macá volcano eruption MAC1 dated at 550 ± 60AD (Naranjo and Stern, 2004). Moreover, the chemical composition of the glass shards retrieved from this main tephra layer in both cores LEs14 and LEs11 fall within the field of Low Abundance Magma Field (LAMF), a chemical signature consistent with the

few measured compositions of MAC1-related glass shards (Figure 4). The median age (~1699 AD) of tephra layer T2 (18.2-18.4 cm) is consistent with the historical eruption of the Mentolat volcano MEN1710 (Siebert et al., 2010). Such origin also agrees with its VLAMF to LAMF chemical signature (Figure 4). The age of deposition for tephra layer T6 estimated ca 168-178 AD (median-mean) is consistent Hudson HU2200 eruption (2.2 kyr ^{14}C, 300AD-140BC). This correlation is also supported by the HAMF-type chemical signature of T6 glass shards ranging in the field defined for the Hudson HU2200 eruption (Naranjo and Stern, 2004; Kratzmann et al., 2010) from basaltic to siliceous andesites (Figure 4). Likely the tephra layer T11 (median ~1373 BC) is also characterised by a Hudson-like signature (HAMF) within the field of K-rich siliceous andesites, consistent in particular with the Hudson H2/T5 eruption (HU3600 BP, 1875±235 BC, Naranjo and Stern, 2004 - Figure 4).

[insert Table 3]

The Lake Esponja sediments record additional tephra layers (Figure 4) that probably correspond to minor eruptions not reported in literature. The tephra layer T1 (13.2-13.5 cm, median 1852 AD) and T10 (median ~785 BC) display a K_2O-low geochemical signature in the LAMF. Their measured chemical signature is rather consistent with some Macá-related eruption. In addition, the tephra correlation for LEs14 may be compared with lacustrine tephra record in nearby lakes (Table 3). T5 (median 537 AD) is probably equivalent to the tephra deposition CAS-T3 and ESC-T3, respectively identified in Lake Castor and Lake Escondida (see location on figure 1) at an extrapolated age of ~160 AD (Elbert et al., 2013). Weller et al. (2015) already proposed their correlation to MAC1 according to the glass shard chemistry of ESC-T3 that is different than any Hudson-related tephra as reported in Elbert et al. (2013). Likely T3 (median 957 AD) and T4 (median 780 AD) are correlated to the tephra deposition CAS-T1/ESC-T1 (950AD) and CAS-T2/ESC-T2 (400AD), respectively. Note these correlations, consistent in age for T3, are not supported by any chemical data for those tephra

layers. T6 (median ~178 AD) and T8 (~246 BC) with their K-rich HAMF type composition may be lateral equivalents of the tephras CAS-T4/CAS-T4 (90AD) and CAS-T6/CAS-T6 (310BC). By stratigraphic interpolation T7 (median ~82 AD) would be related to CAS/T5/ESC-T5 (50BC). T7 probably corresponds to a tephra observed in the Villa-Mañihuales area dated at 130AD (Energia Austral Ltda 2012 cited in Mella et al., 2012) and associated to the volcanic complex Maca-Cay. Finally, the chemical signature of the oldest tephra observed in LES14 T11 is consistent with the K-rich and Si-rich composition of CAS-T8 that was correlated to Hudson H2/T5 eruption (Elbert et al., 2013). The correlation is supported by both the peculiar chemical signature of CAS-T8, even its median interpolated age (~1373 BC) is younger. The Hudson H2 tephra has also been recorded in the sediments of Lake Unco (see location in Figure 1, data from Weller et al., 2014).

5.3. Paleolacustrine and paleoenvironmental conditions

The evolution of the diatom assemblages in LEs14 is reported according to core depth respect to with PC1 and a selection of geochemical ratios (Figure 7). Si/Al, Zr/Rb, Br/Ti and Ca/Ti are used as proxies for fine, coarse or organic-rich detrital matter or volcanic supplies, respectively. The overall depth evolution of benthic diatom assemblages in Lake Esponja, detailed in LEs14, evidences pronounced changes in the lake conditions (depth, turbidity, water chemistry) over the last ≤ 3.5 kyr. Such environmental evolution mostly reflects the weathering intensity within the lake watershed, controlled by (1) tectonic and/or (2) climate-driven changes（Battarbee et al., 2001).

[insert Figure 7]

5.3.1. Tectonic control

The Ca/Ti and Zr/Rb curves display pronounced and sharp peaks that mostly coincide with the sedimentary tephra record. However, the presence of several tephra layers along the sediment core does not reflect significative changes in the diatom assemblage in LEs14 as

observed for other Chilean lakes (e.g. Lake Galletué 38°S - Cruces et al., 2008; Laguna del Maule, 36°S - Carrevedo et al. 2015). Tephra deposition and their reworking in the catchment supplies a continuous addition of nutrients to the lake that sustains the lake productivity and in particular diatom growth. However, in Lake Esponja, this was only obvious in the main tephra T5, where the *Aulacoseira* – *Surirella* association (> 40%) emphasizes a marked increase in nutrients and less transparency than in previous stages. Besides, the presence of *Aulacoseira ambigua* inside the tephra indicates that this deposit was not enough to avoid its development, a behavior that has been also observed in central Andes (Frugone-Alvarez et al, 2020).

The major change in diatom assemblage, i.e. the replacement of planktonic taxa by benthic ones (DZ3), was probably due to the closure of the Lake Esponja as a consequence of a major earthquake-induced rupture occurring along the Río Mañihuales Fault and regionaly related to LOFZ. This significative change occurred after a medium sand interval (CL) between 60.1 and 65.7 cm (63 BC-345 AD, best age 166 AD), characterized by relatively high Zr/Rb and Ca/Ti ratios, indicates a high detrital supply, characteristic of rapid sedimentation event related to watershed perturbation and further sediment remobilisation.

The age of this massive interval may be compared with a density-flow deposit (i.e. event SL-F) observed in the Aysén fjord sedimentation (Van Daele et al., 2013). Particularly, SL-F event was dated at ~ 30BC/100AD in Wils et al. (2018) and based on a probabilistic approach the interpretation of the seismic-reflection data gave evidence that this event occurred on the same fault as the 2007 earthquake (Vanneste et al., 2018). According to the same study, the prehistorical earthquakes of the Aysén Fjord most likely had a low to moderate magnitude < 6.5 as expected for crustal earthquakes. The SL-F event was even larger with an estimated magnitude of 6.5 (Vanneste et al., 2018). The most likely ruptures are generally situated on the closest faults to the Aysen fjord, i.e. the Quitralco, Azul Tigre or Río Mañihuales Faults (Vanneste et al., 2018). According to the revised age model of Wils et al. (2020), SL-F event

includes two partial earthquake ruptures occurring at AD~15 and AD~100, the oldest one affected the southern part of the Valdivia segment (i.e. the closest to Lake Esponja location) whereas the youngest one only ruptured along its northern segment. The purely detrital mineralogy of sample 66-67 cm (Figure 3) could record the inception of the massive event, its age being consistent with the major tectonic event SL-F (Wils et al. 2020) in Aysén fjord. The mineralogy of the coarse sandy interval 60-65.7 cm evidences the contribution from reworked tephra (T7) as observed in Aysén fjord (Van Daele et al., 2013).

5.3.2. Climate control

The geochemical ratios, and in particular Si/Al ratio, have been compared to CRU meteorological data to identify any climate control. For the twentieth century, the evolution of Si/Al ratio in LEs14 displays a significant Pearson correlation (0.70, $p < 0.001$) with austral winter CRU precipitation data, the highest correlation being obtained with a 7-year average (SM Figure 4). The lowest Si/Al values ranging between 6 and 7 ca 1925, 1960 and 1990 AD are roughly consistent with the lowest winter precipitation (~135 mm). Likely the highest Si/Al values (8-10) coincide with the highest winter precipitation comprised between ~170 and 210 mm (ca 1905, 1940, 1968 and 1998 AD). The austral winter precipitations probably enhance weathering processes within the watershed leading to more surface runoff along the lake margins and remobilisation of the Quaternary alluvial formation along the margin. The remobilised particles may then be selectively transported according to grain size, the finest particles settling down in the farthest location. Such observation evidences that the fine detrital supplies, distributed along PC1 axis, are controlled by winter precipitation intensities. The Si/Al ratio may therefore be used in LEs record as a proxy for paleoprecipitation.

[Insert SM Figure 4]

Along of the LEs14 record, the Si/Al ratio profile shows a slightly change at ~ 80-75 cm (200BC – 90BC). Before 80 cm (< 200 BC) high Si/Al ratio values and high variability

suggested high winter precipitation and a resulting increase of the lake level and turbid waters, possibly favoured with the connection of the river Mañihuales. The dominance and high variability of *Aulacoseira* and *Staurosira* confirm these lake conditions with water turbulence and coastal areas dominated by circumneutral to alkaline conditions in the context of a tendentially deep lake as observed in Laguna de Maule, central Chile (Carrevedo et al., 2015). ~~The dominance and high variability of two tycoplanktonic diatoms (*Aulacoseira, Staurosira*) confirms these lake conditions because its planktonic characteristic depends on water turbulence (Bicudo et al. 2016).~~ This predominating wet period has been recognized in pollen sedimentary record from Lake Guanaco (Moreno et al., 2009) associated to an intensification of the SWW.

The Si/Al values decrease after 75 cm would be related to less winter precipitation and therefore a reduced water input from the river and/or the watershed. Calm water conditions were favourable expansion of benthic diatoms, mainly *Surirella*, a genus that lives in shallow environments with high silica requirement (Matteuzzo et al., 2015). The predominance of benthic diatoms in the assemblage for the upper part of the core (Fig. 6), added to sedimentological changes (Fig. 2), could corroborate a main tectonic control, with lesser climatic control reflected in discrete variations in the relative abundance of benthic diatoms and the sudden occurrence of *Aulacoseira* spp.

5.3.3. Environmental evolution

The punctual tectonic and climatic controls being identified in the LEs14 sedimentological and geochemical record, the overall interpretation of the three identified diatom zones is summarized in the next section.

(1) The lower part of LEs14 (i.e. diatom zone DZ1 154-80 cm, ~ 2 kyr BC to 140 BC - Fig. 6) was dominated by tycoplanktonic diatoms (i.e., *Aulacoseira ambigua, Aulacoseira aff. ambigua, Staurosira construens*) associated with ≤ 5% of neutrophil diatoms (i.e. *Cyclotella*

group), consistent with a pH-optimum of ~7-7.4 (Van de Vijver et al., 2002). The association of *Aulacoseira*, *Cyclotella* and *Staurosira construens* suggests eutrophic conditions in a relatively deep but turbid lake (Witak et al., 2017). The abrupt fluctuations in the abundance of *Aulacoseira* and *Staurosira* observed in DZ1a (100-154 cm, 600-2000 yrs BC) give place to an increase of epiphytic diatoms like *Cymbella* and *Epithemia* in the upper part of this interval (DZ1b 80-100 cm, ~200-520 BC). The main change in the diatom composition occurs in the transition interval between DZ1 and DZ2 (DZ1b) where the fragilarioid taxa *Staurosira* and *Aulacoseira* were replaced by *Surirella* taxa. *Staurosira* has been observed in shallow coastal habitats of deep lakes characterized by fairly long seasonal lake-ice cover (Fernandez et al, 2013). Consistent with temperature optima in Canadian artic lakes fragilarioid group is present in cold summer air temperatures (Finkelstein and Gajewski, 2008). *Aulacoseira* kept in the water under turbulent conditions favoured by strong winds and meltwater discharges.~~*Staurosira*, an alkaline preference taxon, suggests warmer conditions (Finkelstein et al., 2008).~~ Lower abundance of *Cyclotella* and sharp fluctuations in the *Aulacoseira-Staurosira* indicate shorter ice cover periods and increased thermal stratification in the lake. The dominance of *Surirella* in DZ1b indicates a change to slightly acidic and mesohalobe waters, low nutrients concentration and high light availability in the lake (Morais et al., 2018), suggesting variations in the water level that trend towards a slight decrease. A similar change has been recognized from other environmental records in a close time window, for both sides of the Andean range, and was related to SWW strength. For example, on the windward side of the Andes, Moreno et al. (2009) recorded in Lago Guanaco a high fire activity associated with a decline in precipitation (650 BC - 350 BC), while on the lee side, a wet period was recognized by changes in floristic composition and fluctuating water levels in Lake Potrok Aike (Kliem et al. 2013, Wille et al. 2007).

The geochemical ratios and PC1 change slowly (Figure 7). A marked change occurs from 58 cm (~230 AD), i.e. just after the sedimentation of the medium sand interval (61-65 cm). Those ratios may record either direct tephra deposition or post-deposition tephra remobilisation that may be important in SVZ due to climate humid conditions (e.g. Fontijn et al., 2014). The Si/Al profile is roughly parallel to Br/Ti fluctuations. Both ratios reflect the weathering conditions in the lake watershed and the variable detrital inorganic or organic supplies.

(2) DZ2 (55-80 cm, ~200 BC-320 AD) is represented by low abundance of benthic moderate acidophilic diatoms (i.e. *Eunotia, Stauroneis and Stenopterobia*), being characteristic of oligo- to mesotrophic conditions. DZ2 is dominated by *Surirella* spp (≤ 99% of abundance - Figure 6). *Surirella* is a common genus semi or loosely attached assigned as benthic but could become planktonic with sufficient turbulence (Bradbury 1997). For instance, this taxon was recorded as planktonic in tropical lakes (e.g. Brazilian reservoir - Morais et al., 2018) characterized by ≥ 10 meters depth, slightly acid water (pH 6), high light availability and low nutrient concentrations corresponding to oligotrophic conditions. At Lake Esponja the presence of this taxon associated to the presence of *Stenopterobia*, a genus also described in the Brazilian reservoirs (Morais et al., 2018), probably recorded similar nutrient-poor conditions. Note the nearly absence or very low content of *Aulacoseira* evidences more water transparency (i.e., low turbid conditions) in the lower part of DZ2a (70-80 cm, ~200 BC - 25 AD) than in previous DZ interval. DZ2a corresponds to an oligosaprophic, oligotrophic, very low alkalinity and calm conditions. The presence of gemmosclere and microsclere sponge spicules (< 20%) observed between 70 and 80 cm is associated to seasonal fluctuations in lake level and high concentration of dissolved Si (Matteuzzo et al., 2015). The presence in sample DZ2b 55-65 cm of *Aulacoseira* records more turbid conditions due to sudden detrital inputs and nutrient availability in the lake. The appearance of *Eunotia* at the

base of DZ2a indicates more acid conditions that will be more steady in DZ3. Volcanic deposits observed along the core caused several changes in redox and pH conditions, increase turbidity and nutrient release that affect the composition in the diatom record including acidification (Kilian et al. 2003). ~~However, diatom communities are observed inside the tephra indicating that volcanic activity was not enough to avoid the diatom development being planktonic *Aulacoseira ambigua* dominating the diatom record. This diatom behaviour has been also observed in central Andes (Frugone-Alvarez et al, 2020).~~

(3) DZ3 (0-57 cm, 255 AD to 2014 AD) shows a remarkable change in environmental conditions in the lake. *Staurosira* disappears from the record and there is an evident shift in *Surirella* and *Aulacoseira*. *Frustulia* spp. and *Eunotia* spp. become characteristic in the upper record and represent benthic acidophilic to acidobiontic species with optimum pH ranging from 3.6 to 6 (De Nicola 2000). *Frustulia* is commonly found in Patagonian lakes and bogs in sites with cold monthly averaged air temperature (4.2°C), acid (3.6 < pH < 5.5) and low dissolved organic carbon (DOC < 20 mg/l^{-1}) waters (Casa et al., 2018). The presence of other epiphytic (*Epithemia*) benthic (*Stauroneis*, *Cymbopleura)* and a decrease of planktonic (*Aulacoseira ambigua*) taxa suggest an expansion of the wetland surrounding the lake and less turbid conditions in a more productive watershed. The common presence (≤ 30%) of *Aulacoseira* and *Eunotia* indicates a closed, more acid environment. This abrupt change in diatom composition with the predominance of *Frustulia* and *Eunotia* may be a consequence of the fault rejuvenation at ~2 kyr BP. The occurrence of phytolites in the last 30 cm of LEs14 record underlines an active erosion around the basin.

Conclusions

The Lake Esponja sediments record a temporal evolution over the last ≤ 3.5 kyr of allochthonous, detrital and volcanic supplies, combined to variable autochthonous contribution in relation with diatom productivity in the water column.

The glass shard major element composition of identified tephra layers gives a record of past major eruptions related to eruptions of regional volcanoes Mentolat (MEN1700), Macá (i.e. MAC1) and Hudson (HU2200, HU2).

The diatom assemblages evidence variable water column conditions in terms of pH, lake depth and turbidity conditions. The dominance of *Aulacoseira* and *Staurosira* emphasizes turbid lake conditions over the first part of the lake evolution (DZ1 150-80 cm, ~2 kyr BC to 140 BC), likely related to the precipitation associated with the SWW variability. The high abundance of *Surirella* marks a change to more stable conditions, with no or low runoff in DZ2a. Within the upper zone (DZ3, 57-0 cm, 255 AD to 2014 AD) *Frustulia* and *Eunotia* underline an evolution of lake conditions towards acid peat environment. This main evolution supports a closure of the lake initiated ~2 kyr ago. Such change may be driven by a rejuvenation of the local Rio Manihuales Fault in relation with a major regional earthquake along the LOFZ tectonic structure and recorded by a massive deposit described in literature in Aysen fjord *ca.* 100AD.

The observed correlation between Si/Al ratio and austral winter precipitation over the twenty century supports that Si/Al may be used, at least for Lake Esponja setting, as a proxy for physical erosion within the watershed. In particular, the higher Si/Al ratios in the lower LEs14 core section (below 80 cm, before 200 BC) record a period of predominantly precipitations leading to a higher lake level and more turbid conditions. Such changes are in agreement with the dominance of *Aulacoseira-Cyclotella-Fragilari*a assemblages in the lower core section. Diatom assemblages are responding to the influence of both volcanic and

tectonic activity deposits modulated by climate variations in this southern part of south hemisphere

Acknowledgements

The authors thank all the persons who contributed for the sample preparation, analyses and/or figure elaboration, in particular I. Billy (UMR EPOC, Université de Bordeaux, France) for XRF core scanner and Scopix measurements, J. Otten from University of Liege for grain-size analysis and Alex Henríquez from the University of Concepcion for the elaboration of the geological map. This research was partially funded by ANID/Fondecyt projects 1201277 and 11201231. D. Álvarez, R. Urrutia and P Pedreros thank to CRHIAM ANID/FONDAP 15130015.

References

Aitchison J (1986) *The Statistical Analysis of Compositional Data*. London: Chapman and Hall.

Appleby PG and Oldfield F (1978) The Calculation of Lead-210 Dates Assuming a Constant Rate of Supply of Unsupported ^{210}Pb to the Sediment. *Catena* 5: 1-8.

Battarbee RW, Jones V J, Flower R J, Cameron NG, Bennion H, Carvalho L, Juggins S (2001) Diatoms. In: Last W M. and Smol J P (eds) *Tracking environmental change using lake sediments*, Volume 3: Terrestrial, Algal, and Siliceous Indicators. Dordrecht, Netherlands**:** Kluwer Academic Publishers, pp.155-202.

Bertrand S, Araneda A, Vargas P, Jana P, Fagel N, Urrutia R (2012) Using the N/C ratio to correct bulk radiocarbon ages from lake sediments: Insights from Chilean Patagonia. *Quaternary Geochronology:* 12, 23-29.

Bertrand S., Hughen K., Sepúlveda J., Pantoja S. (2014) Late Holocene covariability of the southern westerlies and sea surface temperature in northern Chilean Patagonia. *Quaternary Science Reviews*: 105, 195-208.

~~Bicudo D, Tremarin P, Almeida P, Zorzal-Almeida S, Wengrat S, Faustino SB, Costa L, Bartozek E, Rocha A, Bicudo C, Morales E (2016) Ecology and distribution of *Aulacoseira* species (Bacillariophyta) in tropical reservoirs from Brazil, *Diatom Research* 31(3): 199-215, DOI: 10.1080/0269249X.2016.1227376.~~

Bizama G, Torrejón, Aguayo M, Muñoz MD, Echeverría C, Urrutia R (2011) Pérdida y fragmentación del bosque nativo en la cuenca del río Aysén (Patagonia-Chile) durante el siglo XX. *Revista de geografía Norte Grande:* 49, 125-138.

Blaauw MJ Christen A and Aquino Lopez MA (2021) Rbacon: Age-Depth Modelling using Bayesian Statistics. R package version 2.5.3. https://CRAN.R-project.org/package=rbacon.

Bradbury JP (1997) A diatom-based paleohydrologic record of climate change for the past 800 k.y. from Owens Lake, California. *Geological Society of America Special Papers* 317: 99-112. https://doi.org/10.1130/0-8137-2317-5.99.

Bradley RS (1999) Paleoclimatology: reconstruction of climates from the Quaternary. International Geophysics series, 64, Second edition. Academic Press, San Diego, USA. 613 pp.

Candès EJ, Li X, Ma Y, Wright J (2011) Robust principal component analysis? *Journal of Association for computing machinery* 57(8): 1-37.

Carter SJ and Colman SM (1994) Biogenic silica in Lake Baikal sediments: results from 1990-1992 American cores. *Journal of Great lakes Research* 20 (4): 751-760.

Casa V, Mataloni G, Van de Vijver B (2018) Six new Frustulia species (Bacyllariophyta) in Tierra de Fuego peatbogs, Patagonia. Argentina. *Fottea. Olomouc* 18(1): 55-71.

Chapron E, Beck C, Pourchet M, Deconinck JF, (1999) 1822 earthquake-triggered homogenite in Lake Le Bourget (NW Alps). *Terra Nova* 11: 86-92.

Chapron E, Ariztegui D, Mulsow S, Villarosa G, Pino M, Outes V, Juvigné E, Crivelli E (2006) Impact of the 1960 major subduction earthquake in Northern Patagonia. *Quaternary International* 158: 58-71.

Carrevedo ML, Frugone M, Latorre C et al. (2015) A 700-year record of climate and environmental change from a high Andean lake: Laguna del Maule, central Chile (36 S). *The Holocene* 25: 956-972.

Cembrano J, Schermer E, Lavenu A, Sanhueza A (2000) Contrasting nature of deformation along an intra-arc shear zone, the Liquine-Ofqui fault zone, southern Chilean Andes. *Tectonophysics* 319: 129-149.

Cembrano J and Lara L (2009) The link between volcanism and tectonics in the southern volcanic zone of the Chilean Andes: a review. *Tectonophysics* 471: 96-113.

Cembrano J, Hervé F, Lavenu A (1996) The Liquiñe Ofqui fault zone: a long-lived intra-arc fault system in southern Chile. *Tectonophysics* 259: 55-66.

Charrier R, Pinto L, Rodrigues MPM (2007) Tectonostratigraphic evolution of the Andean orogen in Chile. In: Moreno T. and Gibbsons W. (eds.) The Geology of Chile. The Geological Society, London, 21-114.

Croux C, Filzmoser P, Fritz H (2013) Robust sparse principal component analysis. *Technometrics* 55: 202-214.

Cruces F, Urrutia R, Parra O, Araneda A, Treutler H, Bertrand S, Fagel N, Torres L, Barra R. and Chirinos L (2008) Changes in diatom assemblages in an andean lake in response to a recent volcanic event. *Archiv fuer Hydrobiologie* 165(1): 23-35.

Davies SJ, Lamb HF, Roberts SJ (2015) Micro-XRF Core scanning in paleolimnology: recent developments. In: Croudarce IW and Rothwell RG (eds.) *Micro-XRF studies of sediment cores*. Developments in paleoenvironmental Research 17, Springer Science, Dordrecht, 189-226.

Davis JC (2002) Statistics and data analysis in Geology. J. Wiley & sons, New York, 638 pp.

De Nicola DM (2000). A review of diatoms found in highly acidic environments. Hydrobiologia 433, 111-122.

D'Orazio M, Innocenti F, Manetti P, Tamponi M, Tonarini S, González-Ferrán O, Lahsen A, Omarini R (2003) The Quaternary calc-alkaline volcanism of the Patagonian Andes close to the Chile triple junction: geochemistry and petrogenesis of volcanic rocks from the Cay and Maca volcanoes (~45°S, Chile). *Journal of South American Earth Sciences* 16: 219-242.

~~Elbert J, Grosjean M, von Gunten L, Urrutia R, Fischer D, Wartenburger R, Ariztegui D, Fujak M (2012) Quantitative high-resolution winter (JJA) precipitation reconstruction from varved sediments of Lago Plomo 47S, Patagonian Andes, AD 1530-2001. *The Holocene* 22: 465-474.~~

Elbert J, Wartenburger R, von Gunten L, Urrutia R, Fischer D, Fujak M, Hamann Y, Greber N.J, Grosjean M (2013) Late Holocene air temperature variability reconstructed from the sediments of Laguna Escondida, Patagonia, Chile (45°30'S). *Palaeogeography, Palaeoclimatology, Palaeoecology* 369: 482-492.

Fagel N, Alvarez D, Namur O, Devidal JL, Nuttin L, Schmidt S, Jana P, Torrejon F, Bertrand S, Araneda A and Urrutia R (2017) Lacustrine record of last millennia eruptions in Northern Chilean Patagonia (45-47°S). *The Holocene* 1-25. https://doi.org/10.1177/0959683616687.

Fernandez M, Bjorck S, Wohlfarth B, Maidana N I, Unkel I, Van der Putten N. (2013) Diatom assemblage changes in lacustrine sediments from Isla de los Estados, southernmost South America, in response to shifts in the southwesterly wind belt during the last deglaciation. *Journal of Paleolimnology* 50: 433-446.

Filzmoser P, Fritz H, Kalcher K (2018) pcaPP: Robust PCA by Projection Pursuit. R package version 1.9-73. https://CRAN.R-project.org/package=pcaPP.

Finkelstein SA and Gajewski K (2008) Responses of Fragilarioid-dominated diatom assemblages in a small Arctic lake to Holocene climatic changes, Russell Island, Nunavut, Canada. *Journal of Paleolimnology* 40:1079-1095.

Folk RL and Ward WC (1957) A study in the significance of grain-size parameters. *Journal of Sedimentary Petrology* 27: 3-26.

Fontaine CM, Siani G, Delpech G, et al. (2021) Post-glacial tephrochronology record off the Chilean continental margin (~41°S). Quaternary Science Reviews 261, 106928.

Fontijn K, Lachowycz SM, Rawson H, Pyle DM, Mather TA, Naranjo JA, Moreno-Roa H (2014) Late Quaternary tephrostratigraphy of southern Chile and Argentina. *Quaternary Science Reviews* 89: 70-84.

Frugone-Álvarez M, Latorre C, Giralt S, Polanco-Martínez J, Bernárdez P, Oliva-Urcia B, Maldonado A, Carrevedo ML, Moreno A, Delgado Huertas A, Prego R, Barreiro-Lostres F, Valero-Garcés B (2017) A 7000-year high-resolution lake sediment record from coastal central Chile (Lago Vichuquén, 34°S): implications for past sea level and environmental variability. *Journal of Quaternary Sciences* 32: 830-844.

Frugone-Álvarez M, Latorre C, Barreiro-Lostres F, Giralt S, Moreno A et al. (2020) Volcanism and climate change as drivers in Holocene depositional dynamic of Laguna del Maule (Andes of central Chile - 36°S). *Climate of the Past* 16: 1097-1125.

Garreaud RD, Lopez P, Minvielle M, Rojas M (2013) Large-scale control on the Patagonian climate. *Journal of Climate* 26: 215-230. https://doi.org/10.1175/JCLI-D-12-00001.1.

Garrett RG (2018). rgr: Applied Geochemistry EDA. R package version 1.1.15. https://CRAN.R-project.org/package=rgr.

Gilli A, Ariztegui D, Anselmetti FS, et al. (2005) Mid-Holocene strengthening of the Southern Westerlies in South America - Sedimentological evidences from Lago Cardiel, Argentina (49°S). Global planetary Change 49, 75-93.

Grimm EC (1991) TILIA and TILIA GRAPH. Illinois State Museum, Springfield.

Grimm EC, Maher Jr LJ, Nelson DM (2009) The magnitude of error in conventional bulk-sediment radiocarbon dates from central North America. *Quaternary Research* 72 (2): 301-308.

Gutiérrez F, Gioncada A, González-Ferrán O, Lahsen A, Mazzuoli R (2005) The Hudson volcano and surrounding monogenetic centres (Chilean Patagonia): an example of volcanism associated with ridge-trench collision environment. *Journal of Volcanology and Geothermal Research* 145: 207-233.

Gyuard H, Chapron E, St-Onge G, Anselmetti FS, Arnaud F, Magand O, Francus P, Mélières MA (2007) High-altitude varve records of abrupt environmental changes and mining activity over the last 4000 years in the Western French Alps (Lake Bramant, Grandes Rousses Massif). *Quaternary Science Reviews* 26: 2644-2660.

Harris IC and Jones PD (2020) CRU TS4.03: Climatic Research Unit (CRU) Time-Series (TS) version 4.03 of high-resolution gridded data of month-by-month variation in climate (Jan. 1901- Dec. 2018). Centre for Environmental Data Analysis, *22 January 2020*. doi:10.5285/10d3e3640f004c578403419aac167d82.

Hartley B, Barber HG, Carter JR and Sims PA (1996) An atlas of British diatoms Bristol: Biopress Ltd.

Haberle SG and Lumley SH (1998) Age and origin of tephras recorded in postglacial lake sediments to the west of the southern Andes, 44°S to 47°S. *Journal of Volcanology and Geothermal Research* 84: 239-256.

Hedges JI and Stern JH (1984) Carbon and nitrogen determinations of carbonate-containing solids. *Limnolology and Oceanography* 29(3): 657-663.

Heiri A, Lotter F and Lemcke G (2001) Loss on ignition as a method for estimating organic and carbonate content in sediments: Reproducibility and comparability of results. *Journal of Paleolimnology* 25(1): 101–110.

Hepp C, Reyes C, Muñoz R (2018) Análisis de datos históricos de cinco estaciones meteorológicas de la región de Aysén. Boletín Técnico N°365. Instituto de Investigaciones Agropecuarias, Centro de Investigación INIA Tamel Aike, Coyhaique, Aysén-Patagonia, Chile. 200 pp (In Spanish).

Hervé F (1994). The southern Andes between 39j and 44jS latitude: the geological signature of a transpressive tectonic regime related to a magmatic arc. In: Reutter, K.-J., Scheuber, E., Wigger, P.J. (Eds.), Tectonics of the Southern Central Andes. Springer, Berlin, pp. 243-248.

Hickey RL, Frey FA, Gerlach DC, Lopez-Escobar L (1986) Multiple sources for basaltic arc rocks from the Southern Volcanic Zone of the Andes (34°-41°S); trace element and isotopic evidence for contributions from subducted oceanic crust, mantle, and continental crust. *Journal of Geophysical Research* 91:5963-5983.

Hickey-Vargas RL, Moreno-Roa H, López-Escobar L et al. (1989) Geochemical variations in Andean basaltic and silicic lavas from the Villarrica-Lanín volcanic chain (39.5°S): An evaluation of source heterogeneity, fractional crystallization and crustal assimilation.

Hickey-Vargas RL, Sun M, López-Escobar L et al. (2003) Multiple subduction components in the mantle wedge: Evidence from eruptive centers in the Central Southern volcanic zone, Chile. *Geology* 30(3): 199-202.

Hill MO and Gauch HG. (1980). Detrended correspondence analysis: an improved ordination 613 technique. *Vegetation* 42: 47-59.

Hogg AG, Hua Q, Blackwell PG, Niu M, Buck CE, Guilderson T.P Heaton TJ, Palmer JG, Reimer PJ, Reimer RW, Turney CSM. and Zimmerman SRH. (2013) SHCal13 Southern Hemisphere Calibration, 0-50.000 Years cal BP. *Radiocarbon* 55 (4): 1889-1903.

Juggins S. (2017) rioja: Analysis of Quaternary Science Data, R package version (0.9-21). http://cran.r-project.org/package=rioja.

Kalugin I, Darin A, Rogozin D, Tretyakov G (2013) Seasonal and centennial cycles of carbonate mineralisation during the past 2500 years from varved sediment in Lake Shira, South Siberia. *Quaternary International* 290-291: 245-252.

Kanamori H (1977) The energy release in great earthquakes. *Journal of Geophysical Research* 82: 2981-2987.

Kilian R, Hohner M, Blester H, Wallrabe-Adams, Stern C (2003) Holocene peat and lake sediment tephra record from the southernmost Andes (53-55°S). *Rev. Geol. Chile* 30: 47-64.

Kliem P, Buylaert JP, Hahn A, Mayr C, Murray AS, Ohlendorf C, Veres D, Wastegård S, Zolitschka B, the PASADO science team (2013) Magnitude, geomorphologic response and climate links of lake level oscillations at Laguna Potrok Aike, Patagonian steppe (Argentina). *Quaternary Science Reviews* 71: 131-146.

Krammer K and Lange-Bertalot H (1986) Süßwasserflora von Mitteleuropa, Bacillariophyceae Volume 2/1: Naviculaceae. Gustav Fischer Verlag, Jena. 876p.

Krammer K and Lange-Bertalot H (1988) Süßwasserflora von Mitteleuropa, Bacillariophyceae, Volume 2/2: Bacillariacae, Epithemiaceae, Surirellaceae. Gustav Fischer Verlag, Stuttgart, NewYork. 596p.

Krammer K and grimm-Bertalot H (1991a) Süßwasserflora von Mitteleuropa, Bacillariophyceae, Volume 2/3: Centrales, Fragilariaceae, Eunotiaceae. Spektrum Akademischer Verlag Heidelberg, Berlin. 598p.

Krammer K and Lange-Bertalot H (1991b) Süßwasserflora von Mitteleuropa, Bacillariophyceae, Volume 2/4: Achnanthaceae, Kritische Ergänzungen zu Navicula (Lineolatae) und Gomphonema. Gustav Fischer Verlag, Stuttgart, New-York. 497p.

Kratzmann DJ, Carey S, Scasso RA, Naranjo JA (2010) Role of cryptic amphibole crystallization in magma differentiation at Hudson volcano, Southern Volcanic Zone, Chile. *Contributions to Mineralogy and Petrology* 159: 237-264.

Kylander M, Ampel L, Wohlfarth B, Veres D (2011) High-resolution X-ray fluorescence core scanning analysis of Les Echets (France) sedimentary sequence: new insights from chemical proxies. *Journal of Quaternary Sciences* 26: 109-117.

Kylander M, Lind E, Wastegard S, Lowemark L (2012) Recommendations for using XRF core scanning as a tool in tephrochronology. *Holocene* 22: 371-375.

Lange-Bertalot H, Rumrich U, Rumrich M (2000) Diatoms of the Andes (From Venezuela to Patagonia/ Tierra Del Fuego). Iconografia diatomologica. Vol .9.

Legrand D, Barrientos S, Bataille K, Cembrano J, Pavez A (2011) The fluid-driven tectonic swarm of AysenFjord, Chile (2007) associated with two earthquakes (Mw = 6.1 and Mw = 6.2) within the Liquine-Ofqui Fault Zone. *Continental Shelf Research* 31: 154-161.

Leinen M (1977) A normative calculation technique for determining opal in deep-sea sediments. *Geochimica Cosmochimica Acta* 41(5): 671-676.

López-Escobar L, Kilian R, Kempton P, Tagiri M (l993) Petrology and geochemistry of Quaternary rocks from the southern volcanic zone of the Andes between 41°30’ and 46°00’S, Chile. *Revista Geológica de Chile* 20 (1): 33-55. doi: 10.5027/andgeoV20n1-a04.

López-Escobar L, Cembrano J, Moreno H (1995a) Geochemistry and tectonics of the chilean Southern Andes basaltic Quaternary volcanism (37º-46ºS). *Revista Geológica de Chile* 22 (2): 219-234.

López-Escobar L, Parada MA, Hickey-Vargas R et al. (1995b) Calbuco Volcano and minor eruptive centres distributed along the Liquiñe-Ofqui Fault Zone, Chile (41°-42°S): Contrasting origin of andesitic and basaltic magma in the Southern Volcanic Zone of the Andes. *Contributions to Mineralogy and Petrology* 119: 345-361.

Lowe DJ (2011) Tephrochronology and its application: a review. *Quaternary Geochronology* 6: 107-153.

Luebert F and Pliscoff P (2006) Sinopsis bioclimática y vegetacional de Chile. Editorial Universitaria, Santiago.

Markgraf V (1993) Paleoenvironments and paleoclimates in Tierra del Fuego and southernmost Patagonia, South America. *Palaeogeogr. Palaeoclimatol. Palaeoecol.* 102 (1-2): 53-68.

Markgraf V, Bradbury JP, Schwalb A, Burns SJ, Stern C, Ariztegui D, Gilli A, Anselmetti FS, Stine S, Maidana N (2003) Holocene palaeoclimates of southern Patagonia: limnological and environmental history of Lago Cardiel, Argentina (49S). *Holocene* 13 (4): 581-591.

Matteuzzo MC, Volkmer-Ribiero C, Varajão AFDC, Varajão CAC, Alexander A, Guadagnin DL, Almeida ACS (2015) Environmental factors related to the production of a complex set of spicules in a tropical freshwater sponge. *Anais da Academia Brasileira de Ciências* 87 (4): 2013-2029.

Mella M, Ramos A, Kraus S, Duhart P (2012) Datos tefroestratigraphicos de erupciones Holocenas del Volcan Mentolat, Andes del Sur (44°40'S), Chile. *In :* Congreso Geológico Chileno, No. 13, Actas, Antofagasta. doi: 10.13140/2.1.5150.8500.

Moernaut J, De Batist M, Charlet F, Heirman K, Chapron E, Pino M, Brümmer R., Urrutia, R. (2006) Giant earthquakes in South-Central Chile revealed by Holocene mass-wasting events in Lake Puyehue. *Sedimentary Geology* 195(3-4): 239-256.

Moernaut J, Van Daele M, Heirman K, Fontijn K, Strasser M, Pino M, Urrutia R and De Batist M (2014) Lacustrine turbidites as a tool for quantitative earthquake reconstruction: New evidence for a variable rupture mode in south central Chile: *Journal of Geophysical Research-Solid Earth* 119: 1607-1633, https://doi.org/10.1002/2013JB010738.

~~Moernaut J, Van Daele M, Fontijn K, Heirman K, Kemp P, Pino M et al. (2018). Larger earthquakes recur more periodically: New insights in the megathrust earthquake cycle from lacustrine turbidite records in south- central Chile. *Earth and Planetary Science Letters 481:* 9-19.~~

Moore D and Reynolds RC Jr (1997) *X-Ray Diffraction and the Identification and Analysis of Clay Minerals*. Oxford: Oxford University Press, 332 pp.

Morales EA, Wetzel CE, Rivera SF, Van de Vijver B, Ector L (2014) Current taxonomic studies on the diatom flora (Bacillariophyceae) of the Bolivian Altiplano, South America, with possible consequences for palaeoecological assessments. *Journal of Micropalaentology* 33: 1-9.

Morais KS, Bartozek ER, Zorzal-Almeida S, Bicudo DC, de Mattos Bicudo CE (2018) Taxonomy and ecology of order Surirellales (Bacillariophyceae) in tropical reservoirs in Southeastern of Brazil. *Acta Limnologica Brasiliensia* 30: 204.

Moreiras SM 2005 Climatic effect of ENSO associated with landslide occurrence in the Central Andes, Mendoza Province, Argentina. *Landslides* 2: 53-59.

Moreno PI, François JP, Villa-Martínez RP, Moy CM (2009) Millennial-scale variability in Southern Hemisphere westerly wind activity over the last 5000 years in SW Patagonia. *Quaternary Science Review* 28: 25-38.

Mueller UA and Grunsky EC (2016) Multivariate spatial analysis of lake sediment geochemical data, Melville Peninsula, Nunavut, Canada. *Applied Geochemistry* 75: 247-262.

Naranjo JA and Stern CR (1998) Holocene explosive activity of Hudson Volcano, southern Andes. *Bulletin of Volcanology* 59: 291-306.

Naranjo JA and Stern CR (2004) Holocene tephrochronology of the southernmost part (42° 30′-45°S) of the Andean Southern Volcanic Zone. *Revista Geologica de Chile 31* (2): 225-240.

Oksanen J, Blanchet FG, Friendly M, Kindt R, Legendre P, McGlinn D, Minchin P, O'Hara RB, Simpson GL, Solymos P, Stevens M, Szoecs E, Wagner H (2019). vegan: Community Ecology Package. R package version 2.5-6. https://CRAN.R-project.org/package=vegan.

Olhendorf C and Sturm M (2008) A modified method for biogenic silica determination. *Journal of Paleolimnology* 39(1): 137-142.

Oladottir BA, Sigmarsson O, Larsen G et al. (2011) Provenance of basaltic tephra from Vatnajokull subglacial volcanoes, Iceland, as determined by major- and trace-element analyses. *The Holocene* 21: 1037-1048.

Pankhurst R J, Weaver S D, Hervé F and Larrondo P (1999) Mesozoic-Cenozoic evolution of the North Patagonian Batholith in Aysen, southern Chile. *Journal of the Geological Society* 156: 673-694.

Peel M C, Finlayson BL, McMahon TA (2007) Updated world map of the Köppen-Geiger climate classification. *Hydrology and Earth System Sciences Discussions, European Geosciences Union* 4(2): 439-473.

Perren BB, Hodgson DA, Roberts S, Sime L, Van Nieuwenhuyze W, Verleyen E, Vyverman W (2020) Southward migration of the Southern Hemisphere westerly winds corresponds with warming climate over centennial timescales. Communications Earth & Environment 1. https://doi.org/10.1038/s43247-020-00059-6.

R Development Core Team (2018) R: A Language and Environment for Statistical Computing. R Foundation for Statistical Computing, *Vienna, Austria*. ISBN 3- 900051- 07- 0, URL http://www.R-project.org/.

Revelle W (2017) Psych: Procedures for Personality and Psychological Research. North-Western University, Evanston. R package version 1.7.12. URL http://personality-project.org/r/psych.

Sellés D, Rodríguez AC, Dungan MA et al. (2004) Geochemistry of Nevados de Longaví volcano (36.2°S): A compositionally atypical arc volcano in the Southern Volcanic Zone of the Andes. *Revista Geológica de Chile* 31(2): 293-315.

Sepulveda SA, Rebolledo S and Vargas G (2006) Recent catastrophic debris flows in Chile: geological hazard, climatic relationships and human response. *Quaternary International* 158: 83-95.

SERNAGEOMIN (2003) Mapa Geológico de Chile 1:1000000: versión digital. Gobierno de Chile, Servicio Nacional de Geología y Minería, Publicación Geológica Digital, No. 4 (CD-ROM, versión1.0, 2003). Santiago, Chile. 23p.

SERNAGEOMIN (2012) Investigatión geológica minera ambiantal en Aysén (Codigo BIP No. 30036527-0). Resumen ejecutivo y synthesis de localidades. Report, Servicio Nacional de Geología y Minería Santiago, Chile.

Siebert, Simkin T and Kimberly P (2010) *Volcanoes of the World*. 3rd Edition. Berkeley, CA: University of California Press, 568 pp.

Siegenthaler C and Sturm M (1991) Slump induced surges and sediment transport in Lake Uri, Switzerland. Int. Assoc. Theor. Applied Limnology Proceedings 24(2): 955-958.

Stern CR (2004) Active Andean volcanism: its geologic and tectonic setting. *Revista Geologica del Chile* 31(2): 161-206.

Stern CR, de Porras ME, Maldonado A (2015) Tephrochronology of the upper Rio Cisnes valley (44°S), southern Chile. *Andean Geology* 42: 173-189.

Stupar YV, Schäfer J, García MG, Schmidt S, Piovano E, Blanc F, Huneau G, Le Coustumer P (2014) Historical mercury trends recorded in sediments from the Laguna del Plata, Córdoba, Argentina. *Chemie der Erde Geochimistry* 74: 353-363.

Thomson SN (2002) Late Cenozoic geomorphic and tectonic evolution of the Patagonian Andes between latitudes 42°S and 46°S: An appraisal based on fission-track results from the transpressional intra-arc Liquiñe-Ofqui fault zone. *Geological Society of America Bulletin*

114(9): 1159-1173.

Van Daele M, Versteeg W, Pino M, Urrutia R, De Batist M (2013) Widespread deformation of basin-plain sediments in Aysén fjord (Chile) due to impact by earthquake-triggered, onshore-generated mass movements. *Marine geology* 337: 67-79.

Van Daele M et al. (2015) A comparison of the sedimentary records of the 1960 and 2010 great

Chilean earthquakes in 17 lakes: Implications for quantitative lacustrine palaeoseismology. *Sedimentology* 62: 1466-1496, https://doi.org/10.1111/sed.12193.

Van de Vijver B, Frenot Y, Beyens B (2002) Freshwater Diatoms from Ile de la Possission (Crozet Archipelago, Subantartica). Bibliotheca Diatomologica, Volume 46, Cramer, Berlin, 44-46, 147.

Vanneste K, Wils K, Van Daele M (2018) Probabilistic evaluation of fault sources based on paleoseismic evidence from mass-transport deposits: The example of Aysén Fjord, Chile. *Journal of Geophysical Research: Solid Earth* 123: 9842-9865.

Villa-Martinez R, Moreno PI and Valenzuela MA (2012) Deglacial and postglacial vegetation changes on the eastern slopes of the central Patagonian Andes (47°S) Quaternary Science Reviews 32, 86-99.

Waldmann N, Anselmetti FS, Ariztegui D, Austin JAJr, Pirouzn M, Moy C, Dunbar R (2011) Holocene mass-wasting events in Lago Fagnano, Tierra del Fuego (54°S): implications for paleoseismicity of the Magallanes-Fagnano transform fault. *Basin Research* 23: 171-190.

Wang M.J, Zheng HB, Xie X et al. (2011) A 600-year flood history in the Yangtze River drainage: Comparison between a subaqueous delta and historical records. *Chinese Science Bulletin* 56: 188-195.

Watt SFL, Pyle DM and Mather TA (2013) The volcanic response to deglaciation: Evidence from glaciated arcs and a reassessment of global eruption records. *Earth Science Review* 122: 77-102.

Weller D, Miranda CG, Moreno PI, et al. (2015) Tephrochronology of the Southernmost Andean soutertn Volcanic zone, Chile. Bulletin of Volcanology 77: 107.

Weller D, Miranda CG, Moreno PI, Villa-Martínez R, Stern CR (2014) The large late-glacial Ho eruption of the Hudson volcano, southern Chile. *Bulletin of Volcanology* 76: 831.

Wille M, Maidana N, Schäbitz F, Fey ML, Haberzettl T, Janssen S, Lücke A, Mayr C, Ohlendorf C, Schleser G, Zolitschka B (2007) Vegetation and climate dynamics in southern South America: The microfossil record of Laguna Potrok Aike, Santa Cruz, Argentina. *Review of Palaeobotany and Palynology* 146: 234-246.

Wils K, Van Daele M, Lastras G, Kissel, Lamy F, Siani G (2018) Holocene event record of Aysén Fjord (Chilean Patagonia): An interplay of volcanic eruptions and crustal and megathrust earthquakes. *Journal of Geophysical Research: Solid Earth* 123: 324-343.

Wils K, Van Daele M, Kissel C, Moernaut J, Schmidt S, Siani G, Lastras G (2020) Seismo-turbidites in Aysèn Fjord (southern Chile) reveal a complex pattern of rupture modes along the 1960 megathrust earthquake segment. *Journal of Geophysical Research: Solid Earth* 125. https://doi.org/10.1029/2020JB019405 e2020JB019405.

Witak M, Hernández-Almeida I, Grosjean M, Tylmann W (2017) Diatom-based reconstruction of trophic status changes recorded in varved sediments of Lake Żabińskie (NE Poland), AD 1888-2010. *Oceanological and Hydrobiological Studies* 46(1): 1-17.

Żarczyński M, Wacnik A, Tylmann W (2019) Tracing lake mixing and oxygenation regime using the Fe/Mn ratio in varved sediments: 2000 year-long record of human-induced changes from Lake Żabińskie (NE Poland). *Science of the Total Environment* 657: 585-596.

Ziegler M, Jilbert T, de Lange GJ, Lourens LJ, and Reichart GJ (2008) Bromine counts from XRF scanning as an estimate of the marine organic carbon content of sediment cores. Geochemistry Geophysics Geosystems 9: Q05009.

Tables

Sample	Tephra	nb.	SiO2	TiO2	Al2O3	FeO	MnO	MgO	CaO	Na2O	K2O	P2O5	Sum
LEs14 7-8	µT1	6	58.79 ± 5.33	1.14 ± 0.27	16.38 ± 1.78	6.73 ± 0.99	0.16 ± 0.03	2.63 ± 0.93	6.53 ± 2.39	4.24 ± 0.37	1.18 ± 0.22	0.54 ± 0.15	98.32
LEs14 13-14	T1	11	63.27 ± 1.99	0.89 ± 0.22	16.22 ± 1.16	4.44 ± 1.19	0.15 ± 0.05	1.60 ± 0.91	4.75 ± 0.99	5.21 ± 0.46	1.20 ± 0.27	0.41 ± 0.10	98.15
LEs14 18-19	T2	9	66.18 ± 3.20	0.78 ± 0.13	15.33 ± 1.46	4.15 ± 0.74	0.13 ± 0.05	1.24 ± 0.39	3.43 ± 1.02	4.53 ± 0.41	1.68 ± 0.42	0.24 ± 0.09	97.70
LEs14 31-32	T3	11	56.13 ± 0.2	1.68 ± 0.26	14.49 ± 1.35	10.97 ± 1.03	0.21 ± 0.03	3.30 ± 0.44	6.66 ± 0.36	3.88 ± 0.43	0.98 ± 0.13	0.27 ± 0.08	98.58
LEs14 34-35	T4	10	55.98 ± 0.82	1.63 ± 0.20	14.62 ± 0.83	11.03 ± 1.10	0.21 ± 0.03	3.49 ± 0.37	6.78 ± 0.42	3.73 ± 0.47	1.02 ± 0.18	0.28 ± 0.04	98.78
LEs14 48-49	T5	11	62.36 ± 5.59	1.33 ± 0.78	14.39 ± 1.23	7.95 ± 4.39	0.32 ± 0.35	1.88 ± 0.82	4.59 ± 1.61	4.09 ± 0.46	1.44 ± 0.27	0.25 ± 0.16	98.57
LEs14 60-61	T6	14	55.44 ± 1.94	1.65 ± 0.24	15.15 ± 1.2	8.68 ± 0.84	0.18 ± 0.04	3.60 ± 0.88	7.14 ± 0.73	4.39 ± 0.38	1.41 ± 0.28	0.61 ± 0.11	98.27
LEs14 67-68	T7	14	54.22 ± 1.70	1.46 ± 0.14	14.41 ± 0.91	10.04 ± 1.24	0.20 ± 0.03	4.98 ± 0.75	8.27 ± 0.81	3.65 ± 0.45	1.03 ± 0.34	0.33 ± 0.13	98.59
LEs14 73-74	µT2	14	56.45 ± 0.86	1.85 ± 0.39	14.98 ± 1.17	8.88 ± 1.28	0.19 ± 0.03	2.85 ± 0.41	5.95 ± 0.48	4.37 ± 0.24	1.98 ± 0.30	0.76 ± 0.19	98.28
LEs14 79-80	µT3	14	59.53 ± 6.86	1.30 ± 0.45	15.15 ± 0.99	7.62 ± 3.01	0.17 ± 0.06	2.88 ± 1.41	5.69 ± 2.11	4.14 ± 0.37	1.55 ± 0.53	0.33 ± 0.19	98.36
LEs14 82-83	T8	14	55.23 ± 1.31	1.80 ± 0.34	14.96 ± 1.05	9.31 ± 1.74	0.18 ± 0.04	3.32 ± 0.34	6.78 ± 0.63	4.26 ± 0.39	1.50 ± 0.24	0.65 ± 0.14	97.99
LEs14 102-103	T9	15	55.73 ± 0.50	1.70 ± 0.14	13.87 ± 0.64	11.49 ± 0.77	0.22 ± 0.04	3.88 ± 0.31	7.47 ± 0.38	3.38 ± 0.31	0.96 ± 0.13	0.25 ± 0.04	98.96
LEs14 110-111	T10	12	53.66 ± 0.82	1.87 ± 0.16	13.03 ± 0.36	12.61 ± 1.13	0.23 ± 0.03	4.53 ± 0.80	8.43 ± 1.32	3.27 ± 0.34	0.88 ± 0.26	0.39 ± 0.14	98.90
LEs14 148-149	T11	9	59.83 ± 4.83	1.39 ± 0.29	15.42 ± 0.80	7.17 ± 3.38	0.19 ± 0.03	2.33 ± 1.31	5.04 ± 2.86	4.81 ± 0.94	2.08 ± 0.90	0.32 ± 0.04	98.58
LEs11 68-69	T	10	67.32 ± 5.87	0.80 ± 0.58	14.26 ± 1.08	4.85 ± 3.48	0.15 ± 0.05	1.41 ± 1.08	3.83 ± 1.54	4.29 ± 0.54	1.51 ± 0.31	0.14 ± 0.11	98.56
LEs11 73-74	T	5	68.20 ± 0.49	0.58 ± 0.04	15.37 ± 0.50	3.23 ± 0.14	0.14 ± 0.03	0.76 ± 0.13	3.06 ± 0.07	4.79 ± 0.09	1.61 ± 0.04	0.14 ± 0.05	97.84
LEs11 77-78	T	12	64.47 ± 5.83	1.19 ± 0.58	14.25 ± 3.8	6.80 ± 3.44	0.17 ± 0.06	1.67 ± 1.08	4.26 ± 1.65	4.01 ± 0.51	1.56 ± 0.30	0.23 ± 0.10	98.63
LEs11 68-78	*ave.*	*27*	*66.21 ± 5.38*	*0.93 ± 0.58*	*14.46 ± 1.12*	*5.41 ± 3.48*	*0.16 ± 0.05*	*1.41 ± 1.09*	*3.88 ± 1.53*	*4.26 ± 0.56*	*1.55 ± 0.27*	*0.18 ± 0.11*	*98.45*

Table 1 - Microprobe data on glass shards from core LEs14 and three samples retrieved from the main tephra layer in LEs11. Mean data are reported ± 1σ.

Lab. nb.	Core	Sample interval cm	Sample type	Age ^{14}C BP	Range of calendar (calibrated) age 95% confidence level	Organic matter %	C/N %	Reservoir correction year
GdA-3407	LEs11	84-86	macroremain (bivalve)	1890 ± 25	86AD (1.1%) 93AD 113AD (94.3%) 235AD			0
GdA-4034	LEs14	53-54	bulk sediment	1760 ± 24	1704BP (95.4%) 1570BP	13.3	13.0	6
GdA-4035	LEs14	104-105	bulk sediment	3760 ± 30	4220BP (1.1%) 4208BP 4156BP (92.6%) 3966BP 3945BP (1.6%) 3930BP	6.5	13.5	340
GdA-4036	LEs14	107-108	macroremain (charcoal)	2630 ± 26	2773BP (83.7%) 2698BP 2633BP (3.5%) 2616BP 2589BP (7.1%) 2537BP 2528BP (1.1%) 2516BP			0
GdA-4037	LEs14	151-152	bulk sediment	6108 ± 33	7147BP (2.2%) 7127BP 7015BP (93.2%) 6792BP	10.0	15.8	1140

Table 2 - AMS ^{14}C ages from macroremains and bulk sediment of cores LEs11 and LEs14.

Tephra ID	Depth interval cm		Age model AD/BC min	max	median	mean	Glass major chemistry	Magma field	Volcanic eruptions source	name	min	max	mean year AD/BC	age ^{14}C BP
µT1	7.8	8.0	1859	1943	1906	1904	interm. andesite	LAMF						
T1	13.2	13.5	1720	1915	1852	1843	sil. andesite	VL-LAMF	*Mentolat*					
T2	18.2	18.4	1412	1857	1699	1682	K-rich sil. andesite	LAMF	Mentolat	Men1710[1]		1710		
T3	31.5	31.7	563	1436	957	968	interm. andesite	LAMF	*Maca*					
T4	34.8	35.0	482	1268	780	803	interm. andesite	LAMF	*Maca*					
T5	39.5	49.5	357	814	537	552	K-rich sil. andesite	LAMF	Maca	MAC1[2]	610	490	550±60	
T6	60.7	61,0	-65	345	178	168	K-rich andesite	HAMF	Hudson	*HU2200*[2]	*300*	*-140*	*250*	*2200*
T7	67.8	68,0	-183	283	82	74	interm. to sil. andesite	LAMF	*Maca*	*Maca130*[3]			*130*	
µT3	79.3	79.4	-498	96	-185	-190	K-rich sil. andesite	LAMF	?					
T8	81.9	82.3	-534	32	-246	-248	K-rich basaltic andesite	HAMF	Hudson	HU2200[2]	300	-140	-250	2200
T9	102.6	102.9	-779	-345	-587	-583	interm. andesite	HAMF	?					
T10	110.7	111.0	-961	-520	-785	-755	interm. andesite	LAMF	?					
T11	148.6	148.8	-1918	-969	-1373	-1387	K-rich sil. andesite	HAMF	Hudson	H2/T5[2]	-1640	-2110	-1875±235	3600

Table 3. Tephra characterizations and correlation to known regional eruptions.

The numbers in superscript indicate the references for the eruptions: (1) Siebert et al., 2010; (2) Naranjo and Stern, 2004; (3) Energia Austral Ltda 2012 cited in Mella et al., 2012.

Figures

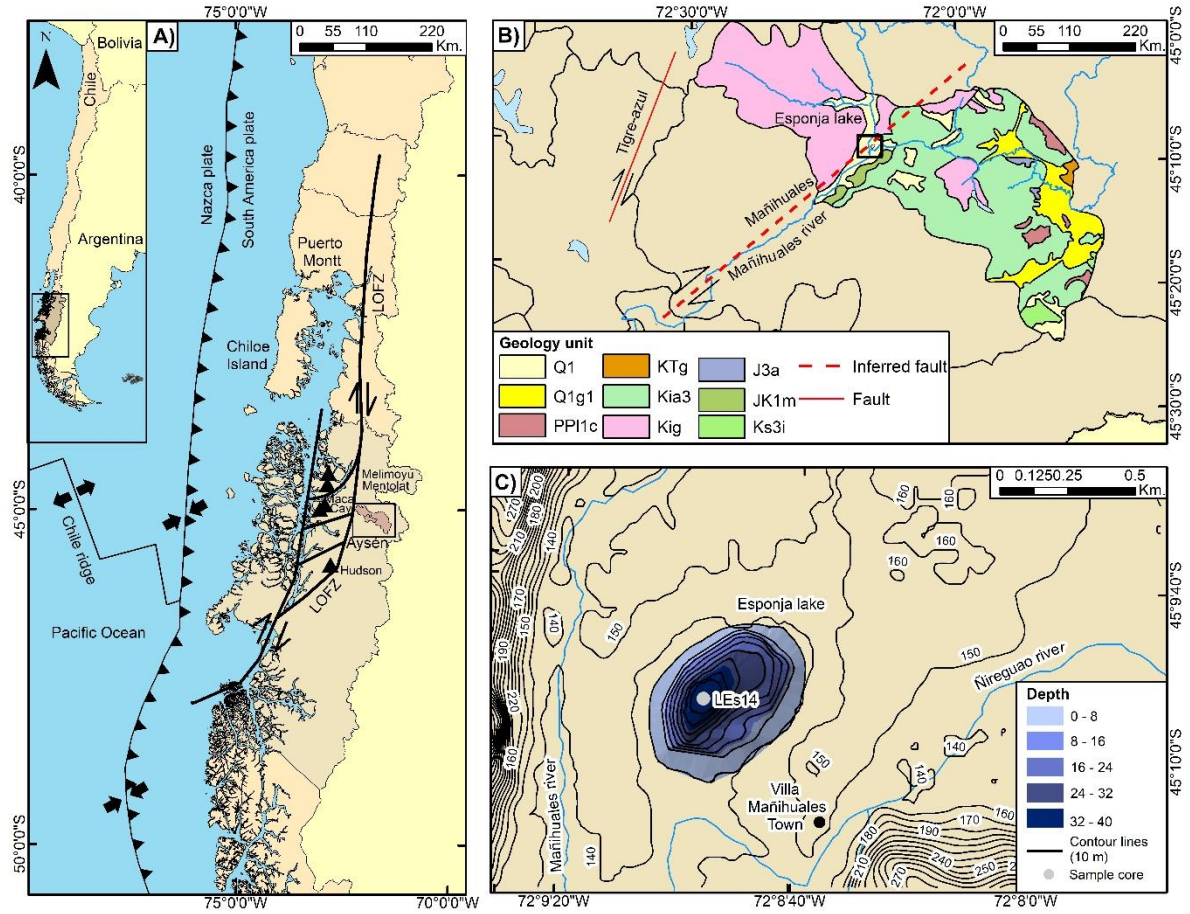

Figure 1 - (a) Location of Lake Esponja within the Aysén region of Chile. The location of the Hudson, Macá, Cay, Melimoyu and Mentolat volcanoes is reported on the map by triangles. (b) Geology of the watershed of Lake Esponja and adjacent watersheds (data from SERNAGEOMIN 2003, http://portalgeominbeta.sernageomin.cl/, consulted on July 2021). The lake watershed is made by three sub-watersheds of 308, 674 and 144 km^2 of superficial, respectively. The lake location is given by the black square. The main geological terranes are Late Jurassic/Cretaceous granites and granodiorites (Kig); dacitic to rhyolitic lavas and pyroclastic deposits of the Late Jurassic Ibanez Formation (J3a) with some marine sedimentary deposits (Jk1m); andesitic to rhyolitic lavas and tuffs of the Early Cretaceous Divisadero Formation (Kia3); Quaternary alluvial deposits (Q1); Plio-Pleistocene alluvial deposits (PPl1c); Morainic, fluvio-glacial and glacio-lacustrine deposits Fluvio-glacial deposits (Q1g1). (c). Topography and bathymetry data of the Lake Esponja surroundings. The dotted red line gives the inferred position of the local fault named "Rio Mañihuales fault" reported in Thompson (2002) and SERNAGEOMIN digital map (SERNAGEOMIN, 2003).

~~(https://geometadatos.wordpress.com/2011/05/16/geologia-de-chile-sernageomin-layer-online/, consulted on July 2021). On the field, the fault is observed on the northwest bank of the River Mañihuales in the area characterized by the greatest escarpment. It is a reverse fault associated to mass removal processes.~~

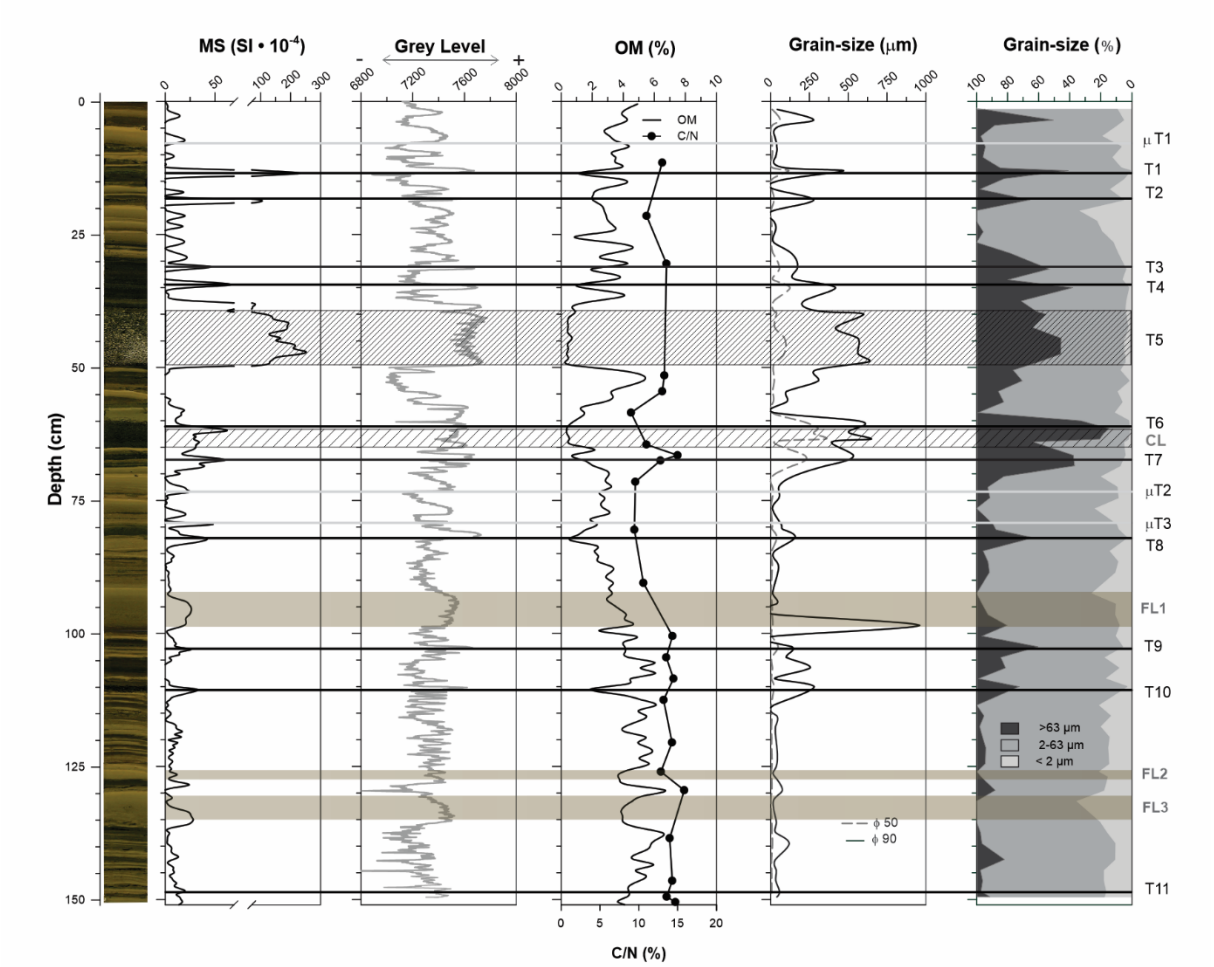

Figure 2 - Detailed sedimentological description of core LEs14 based on physical parameters, i.e. magnetic susceptibility values (MS), SCOPIX grey-scale, organic matter content (from LOI550°C) and C/N ratio and grain-size parameters. The horizontal lines give the position of the tephras whereas the grey lines indicate microtephras. Coarse layer (CL) corresponds to the dashed interval. The three fine turbidites observed in the colour photograph are also reported (FL).

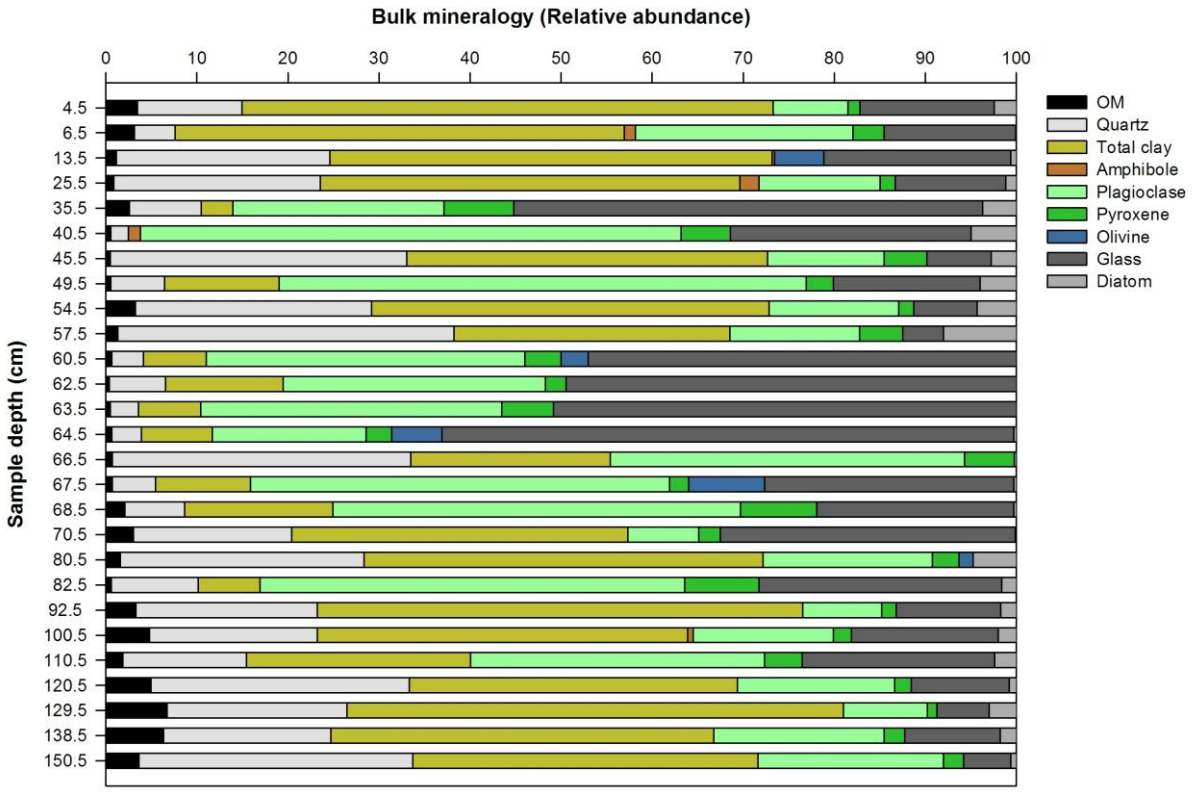

Figure 3. Bulk mineralogy of LEs14 identified by X-ray diffraction on bulk sediment powder (relative abundance**)**.

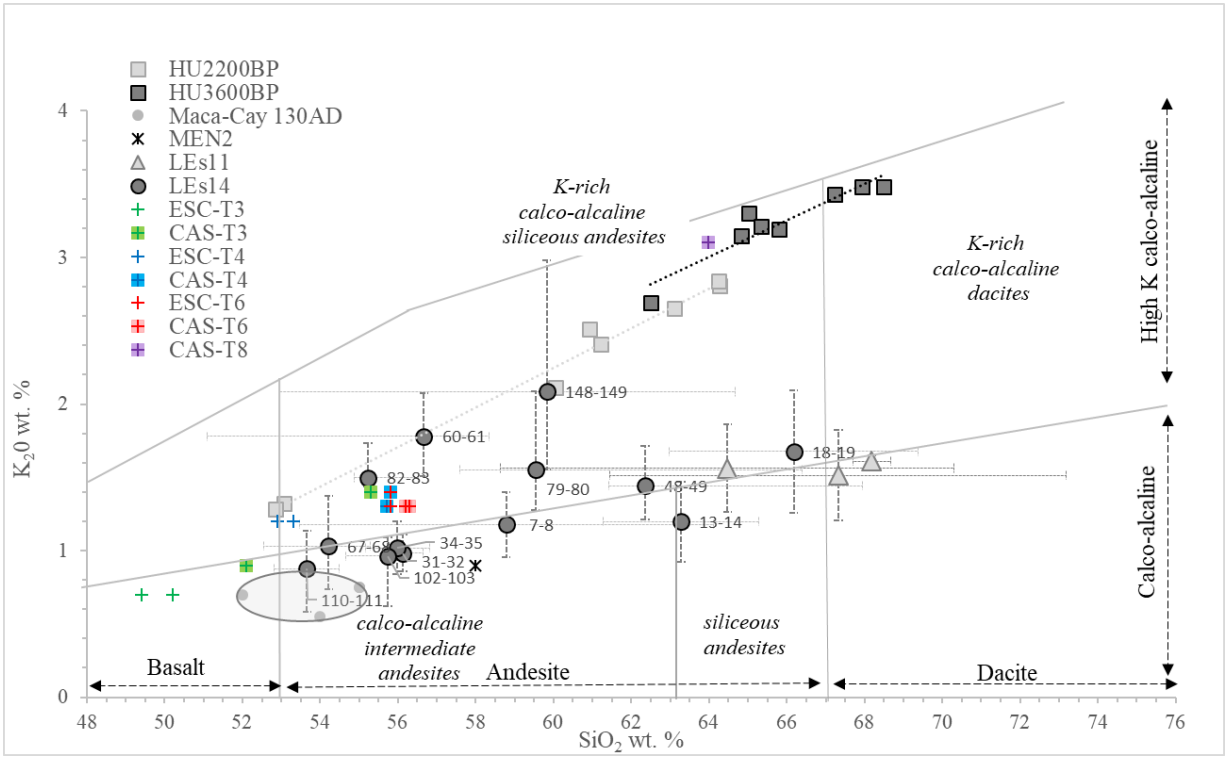

Figure 4 - Averaged major element composition of tephra glass shard samples measured by microprobe and 1σ standard deviation (shaded lines). Data in Table 1. The chemical samples from Chilean Southern Volcanic Zone have previously been termed High, Low and Very Low Abundance magma types (Hickey et al., 1986, 1989, 2003; López-Escobar et al., 1993, 1995a, 1995b; Sellés et al., 2004; Watt et al., 2013). Analyses from historical (MEN1710 - Siebert et al., 2010) and prehistorical eruptions (i.e. MAC 1, HU2200 and HU3600 - Naranjo and Stern, 2004; Maca-Cay 130 AD - Mella et al., 2012) from regional volcanoes are reported for comparison as well as the measured composition of tephra samples retrieved in North Patagonian lacustrine sediments from Lakes Escondida and Castor (Elbert et al., 2013).

Figure 5a. Age model for the upper part of core LEs14 based on ^{210}Pb and ^{137}Cs data measured on LEs13 and transferred by correlation with magnetic susceptibility to LEs14.

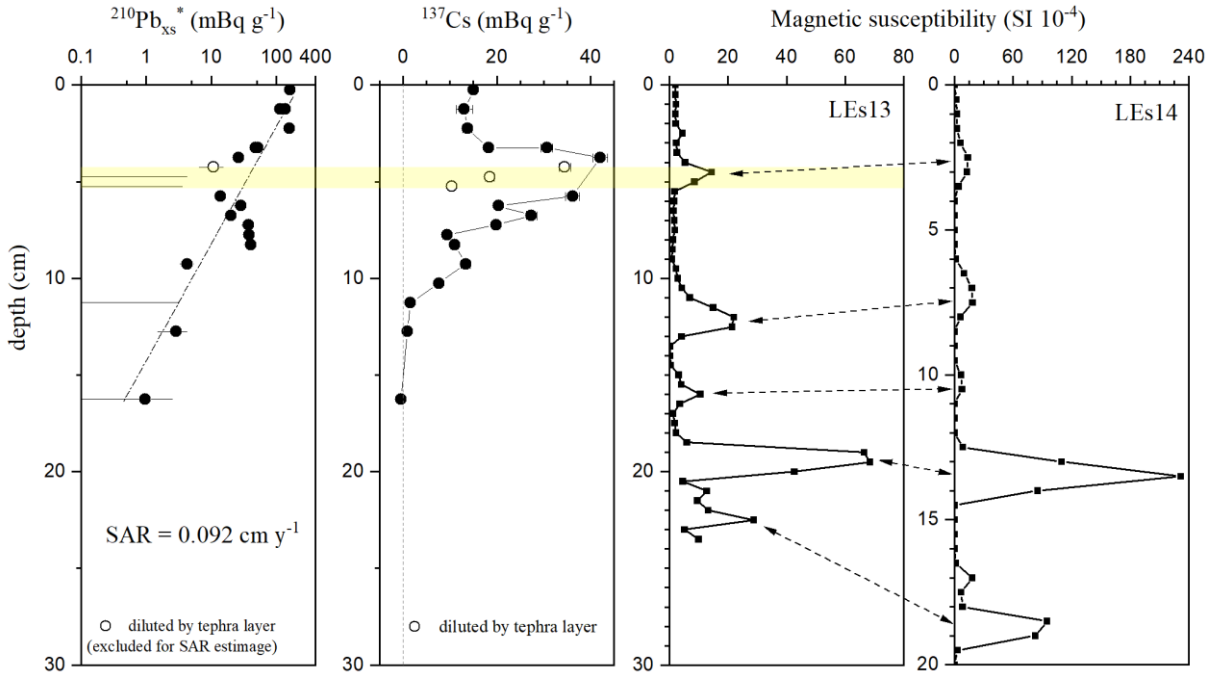

Figure 5b. Age model for the lower part of core LEs14 derived from ^{14}C data reported on Table 2. The horizontal dashed lines correspond to the main tephra layers that have been considered as event deposits (i.e., without any time). Note two age models are compared, with (red line) and without (blue line) considering in account the two ^{14}C ages obtained on bulk sediment at 104.5 and 152.5 cm. Without considering the ages measured on bulk sediments, the Bacon age-depth model indicates that core LEs14 covers 3.5 kyr within 154 cm, with an averaged sedimentation rate of ~0.4 mm/yr, reaching up to 0.6 mm/yr for the upper 10 cm. This age model is consistent with the interval cover by LEs11 estimated from one ^{14}C date measured on a bivalve shell (*Diplodon chilensis*) retrieved between 84 and 86 cm (Table 2).

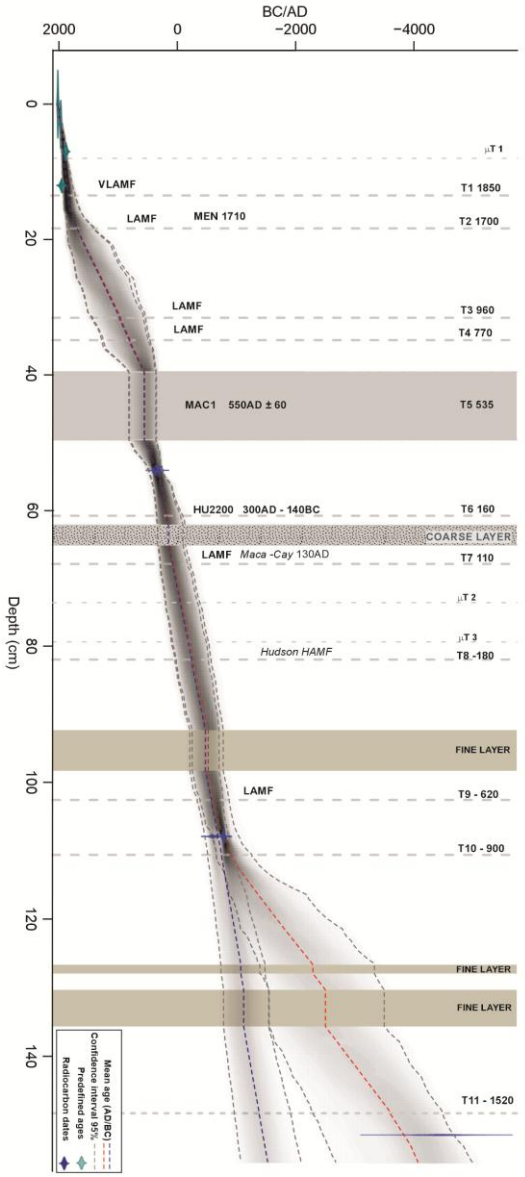

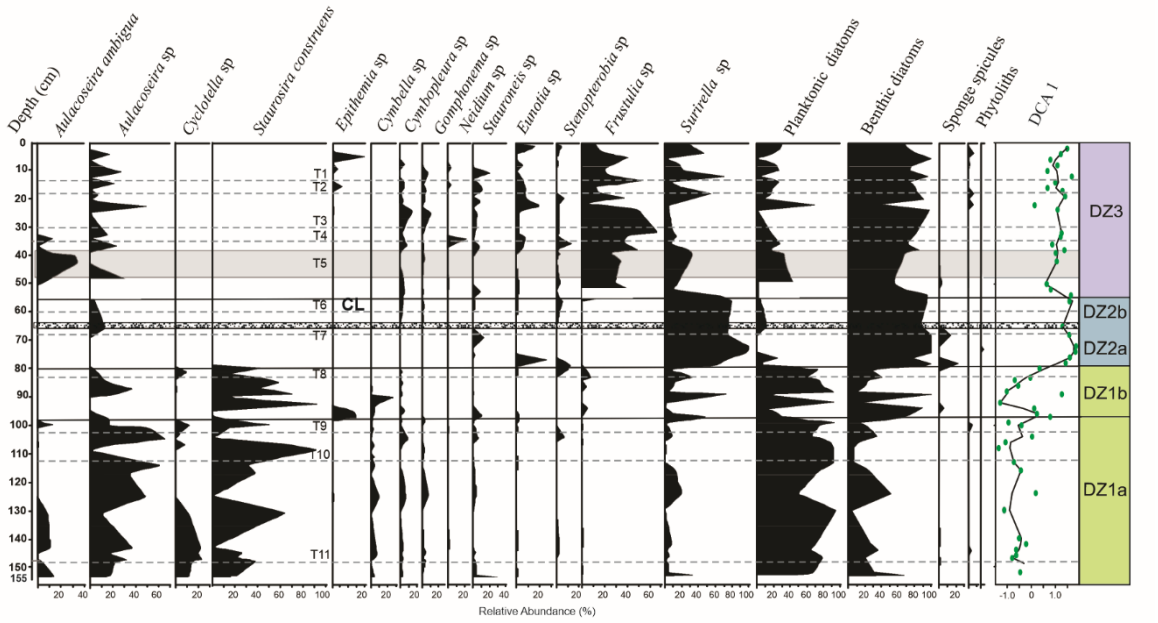

Figure 6 - Diatom assemblages and zonations observed on LEs14.

Figure 7 - Paleoenvironmental synthesis of LEs14 data based on detailed diatom assemblage composition given at Figure 6 and XRF-core scanner data reported as elementary ratios and the first principal component PC1. XRF ratios are presented as ln(Si/Al), ln(Zr/Rb), ln(Br/Ti) and ln(Ca/Ti) indicating fine, coarse or organic-rich detrital matter or volcanic supplies, respectively. The letters reported on the right side of the figure correspond to peculiar layers identified in the core description, i.e. microtephras (µTx), tephras (T), fine turbiditic layers (FLx) and CL coarse layer (CL). The layers are labelled according to the stratigraphical order.

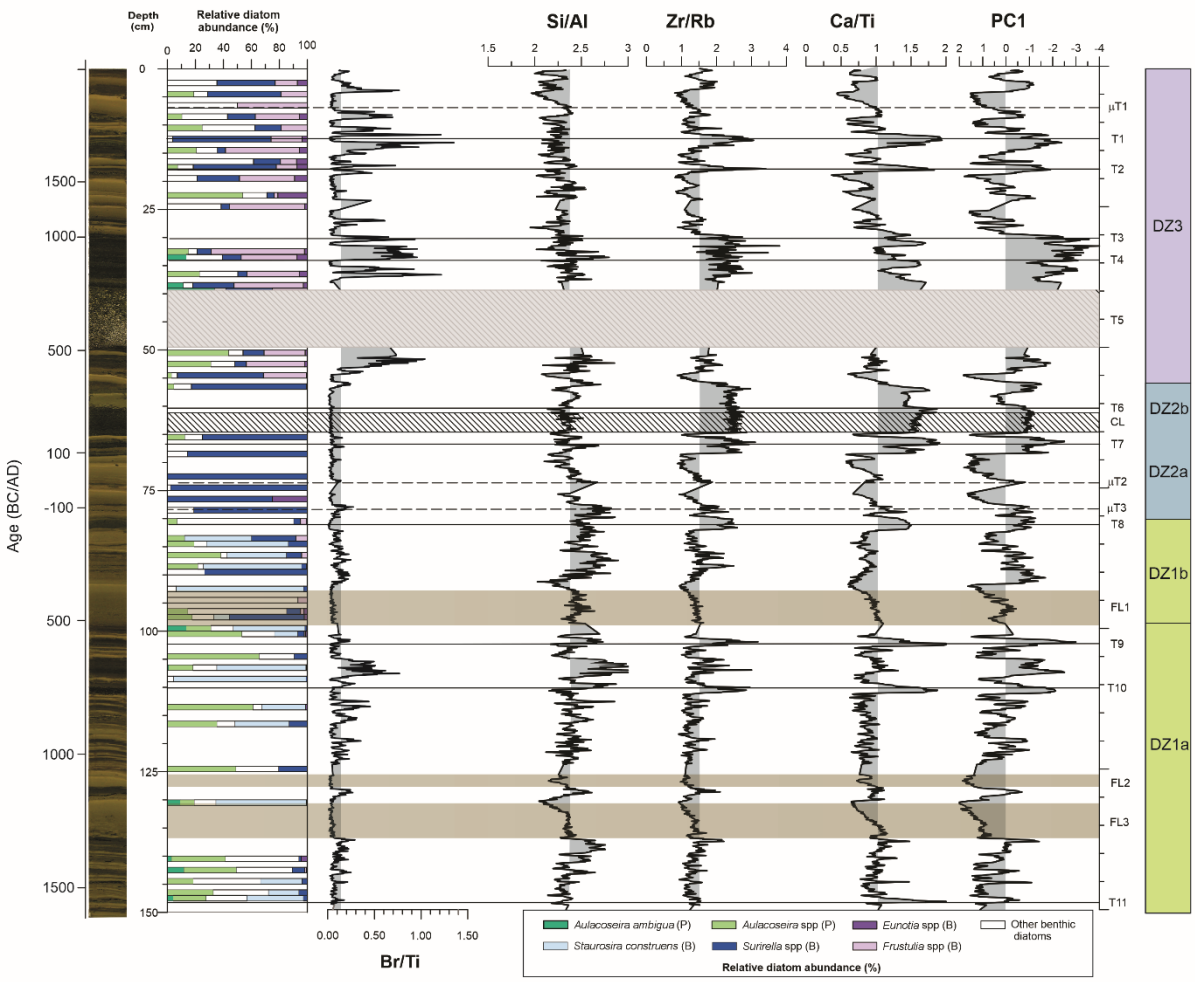

Supplementay figures

SM Figure 1 – Correlation between the cores LEs11A and LEs14. Each core is represented by its SCOPIX X-ray image in grey-scale. The dashed lines give the correlation between the two cores based on the identified peaks of magnetic susceptibility. The letter T indicate the tephra layer. The number I, II and III indicate the main sedimentological units identified in each core. The dotted curve (in green in color version) represents the abundance of biogenic silica in LEs11 as calculated from leaching process.

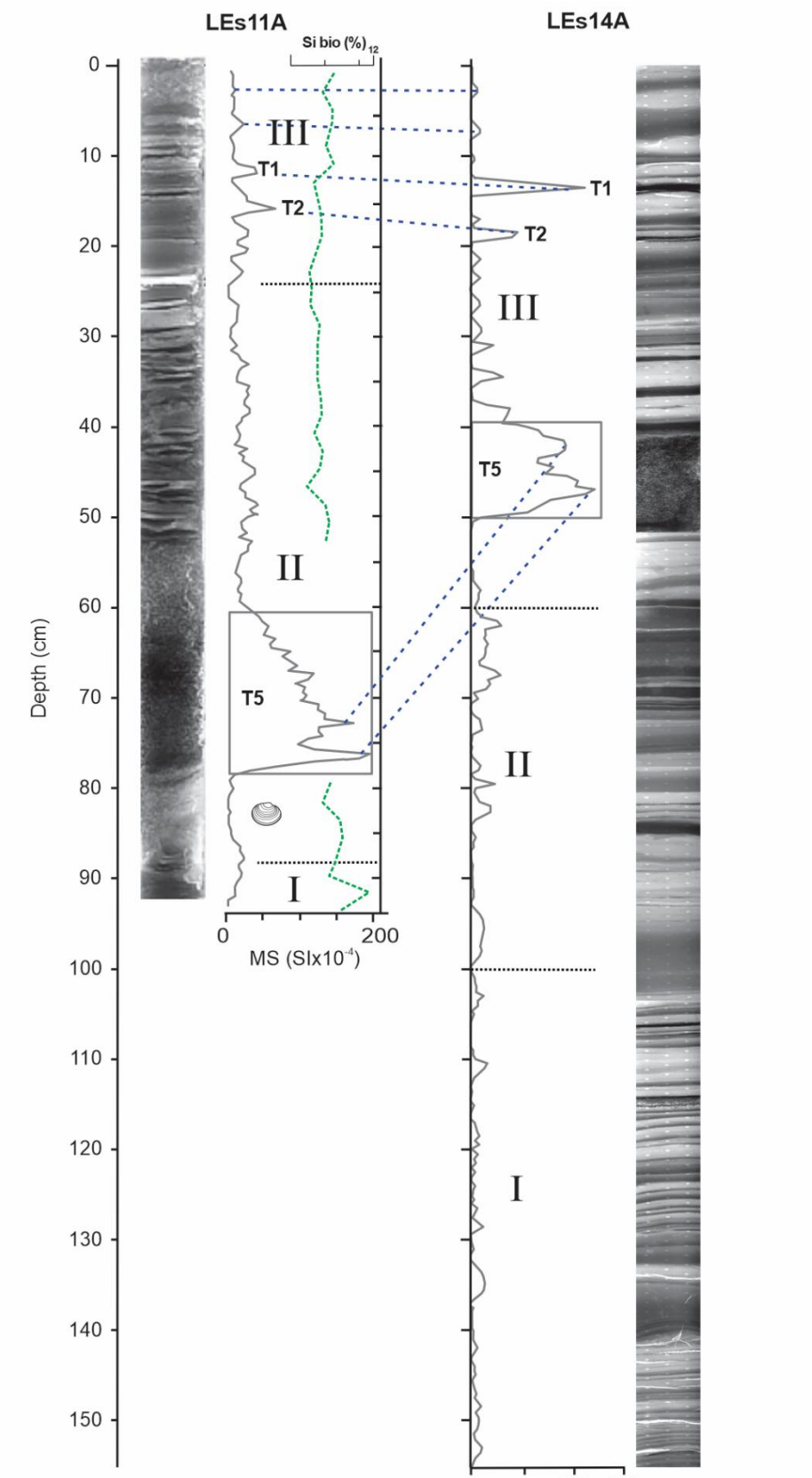

SM Figure 2 - PCA biplot of XRF core scanner dataset of core LEs14 (Lake Esponja, Chile) reported as a binary diagram of the first two principle components PC1 and PC2 (data in SM Table 3).

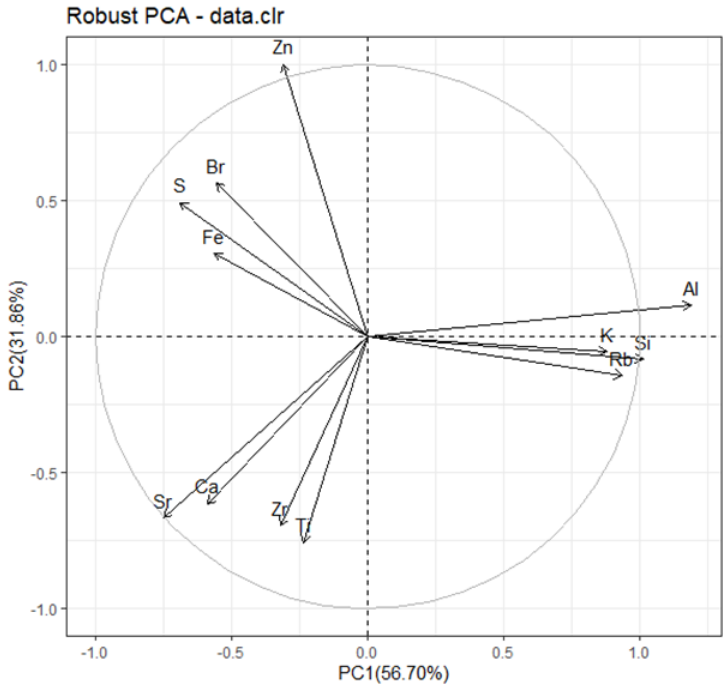

SM Figure 3 - RPCA correlation matrix on XRF core scanner dataset of core LEs14 (Lake Esponja, Chile).

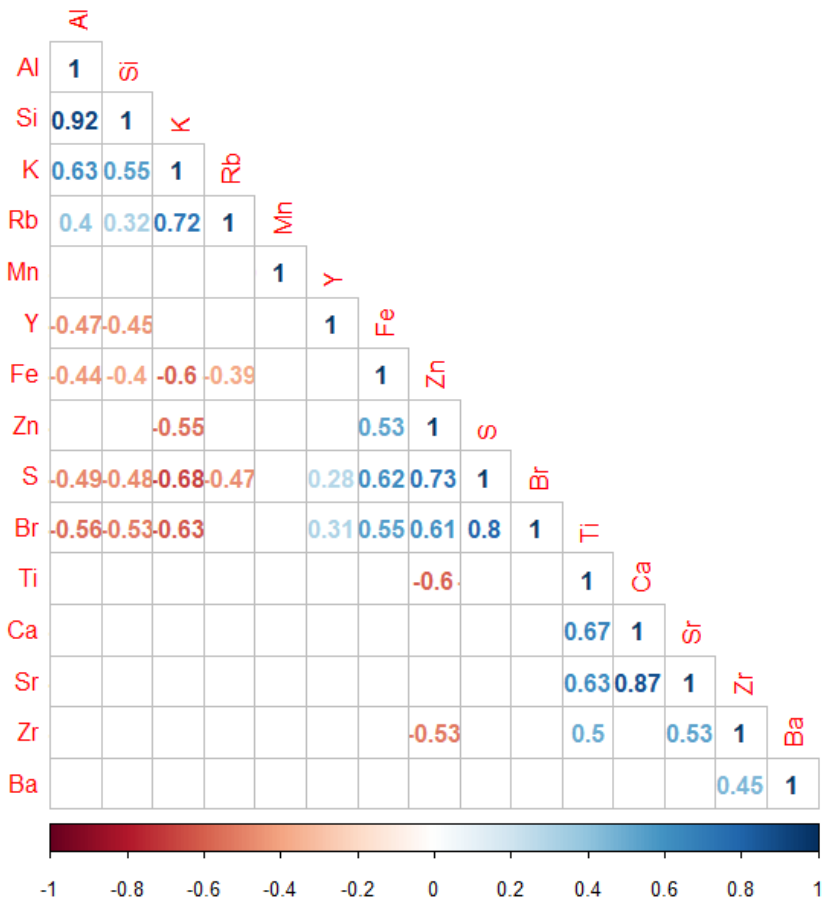

SM Figure 4. Profile of Si/Al ratio calculated from XRF core scanner data compared with 7 years-averaged CRU TS 4.03 winter precipitation data for the 20th century.